LIMNOLOGY
and
OCEANOGRAPHY: METHODS

Limnol. Oceanogr.: Methods 3, 2005, 108–130

New algorithms for MODIS sun-induced chlorophyll fluorescence and a comparison with present data products

Yannick Huot, Catherine A. Brown, and John J. Cullen
Centre for Marine Environmental Prediction, Department of Oceanography, Dalhousie University, Halifax, Nova Scotia, B3H 4J1, Canada

Abstract

We discuss important sources of variability in sun-induced chlorophyll fluorescence and examine difficulties in deriving fluorescence data products from satellite imagery, with a focus on the MODerate-resolution Imaging Spectroradiometer (MODIS) sensor. Our results indicate that there are limitations in the present MODIS algorithms that could lead to biases in the interpretation of the fluorescence products across gradients of chlorophyll concentration. To avoid some of these limitations, we suggest replacing the calculation of absorbed radiation by phytoplankton (*ARP*) over a finite depth with integration over the entire water column, and including a term accounting for cellular reabsorption of fluoresced light. These suggestions are incorporated into two new algorithms, based on established bio-optical models for case 1 waters (most open ocean waters), to retrieve chlorophyll concentration and the quantum yield of fluorescence. We compare our results to the results using MODIS algorithms for two regions: one located off the coast of Central America, including the Costa Rica Dome, and the other in the Arabian Sea. The new algorithms provide a similar field for the quantum yield of fluorescence in the first region, while they provide a different and more uniform field in the second region. We suggest that this discrepancy originates from the use of the water leaving radiance at 412 nm in the MODIS standard algorithm, which is not used in our algorithm and can be problematic under certain environmental conditions (e.g., absorbing aerosols or highly scattering waters).

The launch of the MODIS instrument (Esaias et al. 1998), with a waveband dedicated to the measurement of sun-induced chlorophyll fluorescence, has taken remote sensing of marine phytoplankton in a new direction. In theory, it is now possible to obtain a global quasi-synoptic assessment of near-surface fluorescence emission and its quantum yield. While the remote measurement of in vivo fluorescence emitted by phytoplankton is, in principle, straightforward (but *see* Letelier and Abbott 1996), obtaining an estimate of the quantum yield of fluorescence (the ratio of fluoresced to absorbed photons by phytoplankton) requires a complex algorithm (Abbott and Letelier 1999). Yet, this physiological measurement could foster a major leap in our understanding of the ocean by providing global coverage of a parameter linked to algal physiology (Kiefer and Reynolds 1992) and species composition (Loftus and Seliger 1975; Heaney 1978). In this study, we review the sources of variability of sun-induced fluorescence as they affect the MODIS data products and examine how they relate to the retrieval of the quantum yield of fluorescence and chlorophyll concentration. We propose new algorithms based on semi-empirical relationships from the bio-optical literature and compare our results to MODIS data products.

Nature of the MODIS fluorescence measurement—Quantum yield of chlorophyll fluorescence. In this study, we define the quantum yield of chlorophyll *a* fluorescence in vivo (φ, dimensionless; *see* Table 1 for symbols and definitions) as the ratio of photons fluoresced by chlorophyll *a* over the whole fluorescence band to the photons absorbed by all cellular pigments. Others have referred to this as the apparent quantum yield of chlorophyll *a* fluorescence, limiting the term quantum yield of chlorophyll *a* fluorescence to the ratio of photons fluoresced by chlorophyll *a* (or by chlorophyll *a* associated with photosystem II [PSII]) to those absorbed only by photosynthetic pigments associated with PSII (e.g., Gilmore and Govindjee 1999). This distinction is important for the physiological interpretation of remote sensing data and for the comparison with laboratory measurements (*see* Web Appendix 2).

Acknowledgments

We would like to thank Jasmine Nahorniak and Ricardo Letelier for their help during data processing and interpretation of the MODIS algorithms; Marcel Babin and Douglas Campbell for their thorough comments on an earlier version of the manuscript; Audrey Barnett, Cathy Ryan, and Tara Tapics for their help with manuscript preparation; and Ru Morrison and an anonymous reviewer for their constructive comments on the manuscript. Yannick Huot was supported by NSERC and FCAR scholarships. Research was further supported by CFCAS, NSERC, NRC, NOPP, and ONR.

Table 1. Symbols, definitions, and units

Symbol	Description	Units
a_{gilvin}	Absorption coefficient for colored dissolved matter	m^{-1}
a_f	Attenuation of upwelling fluorescence radiance	m^{-1}
a_φ, a_w	Absorption coefficients for phytoplankton and water	m^{-1}
a_φ^*	Chlorophyll-specific absorption coefficient for phytoplankton	m^2 mg chl^{-1}
$\bar{a}_\varphi^*$	Irradiance-weighted chlorophyll specific absorption coefficient	m^2 mg chl^{-1}
$A_{abs}(z)$	Absorbed radiation per unit volume	mol m^{-3} s^{-1}
ARP	Instantaneous absorbed radiation by phytoplankton	mol m^{-2} s^{-1}
C_f	Proportionality factor, converting fluorescence measurements made at 678 nm to the whole fluorescence band	nm
chl	Chlorophyll a concentration	mg chl m^{-3}
chl_{fluo}	Our estimate of chlorophyll concentration using fluorescence	mg chl m^{-3}
chl_{MODIS}	MODIS estimate of chlorophyll concentration	mg chl m^{-3}
CFE	Chlorophyll fluorescence efficiency: MODIS estimate of φ	unitless
$dL_{em}(z)$	Volume fluorescence emission	mol m^{-3} s^{-1} sr^{-1}
E_{PAR}	Irradiance in the photosynthetically available radiation waveband (400 to 700 nm)	mol m^{-2} s^{-1}
$\mathring{E}(\lambda, z)$	Scalar irradiance	mol m^{-2} s^{-1} nm^{-1}
FLH	Fluorescence line height	W m^{-2} μm^{-1} sr^{-1} *or* mol m^{-2} s^{-1} nm^{-1} sr^{-1}
$ipar$	Instantaneous scalar PAR irradiance just below the sea surface. A standard MODIS algorithm product.	mol m^{-2} s^{-1}
K, K_d, K(PAR)	Attenuation coefficients for scalar, planar, and PAR planar irradiance	m^{-1}
$K_{abs}^{\tau_f}$, $\tilde{K}_{abs}^{\tau_f}$	Fitted attenuation coefficients for absorbed radiation over the depth $z_{\tau f}$ and results of numerical calculation	m^{-1}
L_f	Upwelling radiance due to fluorescence at the surface	mol m^{-2} s^{-1} nm^{-1} sr^{-1}
Q_a^*	Portion of emitted fluorescence not reabsorbed within the cell	unitless
$\beta_\varphi, \beta_{\varphi Q}, \beta_{\varphi aQ}$	Factors applied to the FLH to obtain $\varphi_{est}, \varphi_Q, \varphi_{aQ}$, respectively	mol^{-1} m^{-1} s nm sr mg chl
z	Depth	m
z_{678}	Depth from which fluorescence emission is attenuated by 63.2% at the surface. Used in MODIS algorithm	m
z_{90}	Depth above which 90% of the fluorescence radiance at the surface originates	m
$z_{\tau f}$	Depth above which 63.2% of the fluorescence radiance at the surface originates	m
φ	Real quantum yield of fluorescence in situ	unitless
φ_{chl}	Assumed quantum yield to retrieve chlorophyll concentration from fluorescence: chl_{fluo}	unitless
φ_{est}	Our estimate of the quantum yield of fluorescence	unitless
φ_Q	Coefficient retrieved using FLH and $\beta_{\varphi Q}$; equivalent to a retrieval of the estimated quantum yield if reabsorption within the cell is not accounted for	unitless
φ_{aQ}	Coefficient retrieved using FLH and $\beta_{\varphi aQ}$; variability in this term includes all physiological and species-specific optical influences on fluorescence emission	unitless
λ	Wavelength	nm
θ'	Zenith angle of observation in water	radians

There are three important proximate physiological processes that influence the quantum yield of chlorophyll fluorescence as defined here: (1) photochemical quenching (PQ), (2) nonphotochemical quenching (NPQ) (Krause and Weis 1991), and (3) the fraction of light absorbed by photosynthetic pigments functionally associated with PSII relative to the total light absorbed by the cell. Photochemical quenching is the diminution of φ due to energy flow to photochemical processes (photosynthesis) in competition with fluorescence emission (e.g., Kiefer and Reynolds 1992). With increasing light intensity, photosynthetic systems become saturated and the influence of PQ diminishes, which causes φ to increase. Nonphotochemical quenching is a decline of φ due to competition with nonphotochemical processes (dissipation of energy as heat in the pigment bed or reaction centers). The influence of NPQ is most important at light intensities that are super-saturating

for the photosynthetic systems. Nonphotochemical quenching is a consequence of down-regulation, other photoprotective mechanisms, or damage to photosynthetic reaction centers (Long et al. 1994; Pospisil 1997; Müller et al. 2001).

Polar-orbiting satellites record ocean color data close to midday under cloud-free conditions. Surface irradiance is close to the daily maximum. Also, water absorbs strongly in the red fluorescence waveband, so the depth from which water-leaving fluorescence can be detected is limited to the upper 5 m or so (Babin et al. 1996*b*), where irradiance is also close to maximal. Nonphotochemical quenching is thus important under these midday, clear-sky, near-surface conditions (Maritorena et al. 2000; Morrison 2003) and should be considered directly in the interpretation of fluorescence measured from satellites (Dandonneau and Neveux 1997; Morrison 2003).

Independent of quenching, the fraction of light absorbed by photosynthetic pigments in PSII relative to that absorbed by photoprotective pigments and pigments associated with PSI is directly proportional to the quantum yield (as defined in this study). This is because most chlorophyll fluorescence originates from chlorophyll *a* associated with PSII in vivo. This point is emphasized in Web Appendix 2.

Another factor influencing the observed fluorescence is the reabsorption of fluoresced light within the cell. The fraction reabsorbed varies spectrally and depends on the absorption efficiency of the cell and, therefore, on its size and internal pigment content (Morel and Bricaud 1981; Collins et al. 1985; Morel and Bricaud 1986). This effect has to be addressed to obtain an absolute and accurate measure of φ (Babin et al. 1996*b*).

Furthermore, there are many indirect physiological influences on the quantum yield that affect the magnitude of PQ, NPQ, and the absorption cross-section of PSII as a function of irradiance. These factors include the interaction of incident irradiance (e.g., Kiefer 1973; Kiefer and Reynolds 1992; Kolber and Falkowski 1993; Ibelings et al. 1994) with the species composition (Heaney 1978; Campbell et al. 1998), state of light acclimation (Ögren 1994), and nutritional status (e.g., Kiefer 1973; Cleveland and Perry 1987) of the algal communities.

Since φ is dependent on algal physiological status (Falkowski and Kolber 1995), and physiological responses to environmental variability are adaptive features that can be related to taxonomy (Ibelings et al. 1994; Cullen and MacIntyre 1998), remote sensing of φ could help describe spatial and temporal variability in physiological or trophic status of phytoplankton (depending on the dominant source of variability). While this is true in theory, we still lack the quantitative—perhaps even the qualitative—framework to interpret variability in algal fluorescence under remote-sensing conditions (Cullen and Lewis 1995). More importantly, before physiological interpretations are possible, we need to assess whether remote-sensing images display real variability in φ or simply environmentally driven biases in the algorithms. For this reason, we focus our study on the measurement, rather than interpretation, of the quantum yield of sun-induced chlorophyll fluorescence.

Wavelength of measurement. MODIS measures the upwelling radiance at 676.7 nm (bandwidth 673 to 683 nm, henceforth referred to as the 678 nm waveband), whereas the maximum emission of fluorescence is around 683 to 685 nm. This offset was chosen to avoid an atmospheric oxygen absorption band at 687 nm (Letelier and Abbott 1996; Abbott and Letelier 1999; Gower et al. 2004). In addition to reducing the sensitivity, the offset places the measurement closer to the absorption peak at 676 nm for chlorophyll *a* in vivo, and consequently, measured fluorescence can be reduced by up to 40% by intracellular reabsorption. If the quantum yield is to be obtained accurately, careful corrections are required to account for the absorption of the emitted radiation both inside the cell (Collins et al. 1985; Babin et al. 1996*b*) and within the water column.

Theoretical background—Theoretical descriptions of the oceanic fluorescence field have been published (e.g., Gordon 1979; Preisendorfer and Mobley 1988; Babin et al. 1996*b*; Abbott and Letelier 1999; Maritorena et al. 2000). For completeness, we describe the relationships necessary to estimate the emission of fluorescence near the surface of the ocean from measurements of upwelling radiance.

Neglecting depth variations in φ (assumed to be small in the thin layer from which fluorescence is detected), the infinitesimally small amount of upwelling radiance due to fluorescence at the surface of the ocean (dL_f, mol m^{-2} s^{-1} sr^{-1} nm^{-1}) over a narrow waveband ($\Delta\lambda$, nm) centered at the emission wavelength λ_{em} originating from a thin layer of water at depth z (m) is

$$dL_f(\lambda_{em}, z) = \frac{1}{4\pi} \cdot \frac{\varphi}{C_f} \cdot Q_a^*(\lambda_{em}) \cdot A_{abs}(z) \cdot e^{-a_f(\lambda_{em}) \cdot z} \cdot dz \quad (1)$$

where the factor $1/4\pi$ (sr^{-1}) converts an isotropic fluorescence field to radiance; C_f (nm) is the ratio of the emission in the whole fluorescence band to that observed over $\Delta\lambda$ (assumed independent of reabsorption fraction, but *see* Collins et al. 1985); Q_a^* is a parameter accounting for the fraction of emitted radiation at λ_{em} not reabsorbed within the cell (*see* Babin et al. 1996b); and $A_{abs}(z)$ is the flux absorbed by phytoplankton at depth z (mol m^{-3} s^{-1}). In most case 1 waters, for the MODIS band, the attenuation coefficient for upwelling fluoresced radiance at 678 nm, $a_f(678)$ (m^{-1}), can be approximated as $a_w(678) + a_\varphi(678)$ with a_w and a_φ being the absorption coefficients for water and phytoplankton, respectively (Maritorena et al. 2000). In the remainder of this paper the dependence on λ_{em} = 678 nm is implicit. This description is valid for nadir viewing; for non-nadir viewing conditions, a_f is replaced by $a_f/\cos(\theta')$, where θ' is the zenith angle of observation in water (as defined in Morel and Gentili 1996).

Neglecting variations with depth of the optical properties of phytoplankton and water, the absorbed flux is described by:

$$A_{abs}(z) = \int_{400}^{700} a_\varphi(\lambda) \cdot \overset{o}{E}(\lambda, 0) \cdot e^{-K(\lambda) \cdot z} \cdot d\lambda \quad (2)$$

where $\overset{o}{E}(\lambda, 0)$ (mol m^{-2} s^{-1} nm^{-1}) is the scalar irradiance just below the surface and $K(\lambda)$ (m^{-1}) is the attenuation coefficient.

Integration over depth provides the total amount of fluorescence radiance at the surface:

$$L_f = \frac{1}{4\pi}\cdot\frac{\varphi}{C_f}\cdot Q_a^*\cdot\int_{400}^{700}\int_0^{\infty} a_\varphi(\lambda)\cdot\overset{o}{E}(\lambda,0)\cdot e^{-(K(\lambda)+a_f)\cdot z}\cdot dz\cdot d\lambda$$
$$= \frac{1}{4\pi}\cdot\frac{\varphi}{C_f}\cdot Q_a^*\cdot chl\cdot\int_{400}^{700}\frac{a_\varphi^*(\lambda)\cdot\overset{o}{E}(\lambda,0)}{K(\lambda)+a_f}\cdot d\lambda \quad (3)$$

Here we used $a_\varphi = chl\cdot a_\varphi^*$, where a_φ^* is the chlorophyll specific absorption coefficient for phytoplankton (m^2 mg chl^{-1}).

It is convenient for the formalism presented here to assume a wavelength independent quantum yield. This is rarely the case due to different efficiencies of exciton transfer for different pigment pools and different pigment distributions between PSII and PSI (e.g., Johnsen and Sakshaug 1996; Lutz et al. 1998, 2001), such that φ represents a mean quantum yield weighted by the absorbed irradiance:

$$\varphi = \int_{PAR}\varphi(\lambda)\cdot a_\varphi(\lambda)\cdot\overset{o}{E}(\lambda)\cdot d\lambda \Big/ \int_{PAR} a_\varphi(\lambda)\cdot\overset{o}{E}(\lambda)\cdot d\lambda.$$

Solving Eq. 3 for *chl* and φ gives:

$$chl = \frac{L_f\cdot 4\pi\cdot C_f}{\varphi\cdot Q_a^*}\cdot\left[\int_{400}^{700}\frac{a_\varphi^*(\lambda)\cdot\overset{o}{E}(\lambda,0)}{K(\lambda)+a_f}\cdot d\lambda\right]^{-1}$$
$$\varphi = \frac{L_f\cdot 4\pi\cdot C_f}{chl\cdot Q_a^*}\cdot\left[\int_{400}^{700}\frac{a_\varphi^*(\lambda)\cdot\overset{o}{E}(\lambda,0)}{K(\lambda)+a_f}\cdot d\lambda\right]^{-1}. \quad (4)$$

MODIS algorithms: FLH, ARP, and CFE—Chlorophyll fluorescence efficiency (*CFE*, unitless) is obtained by dividing an estimate of the amount of fluoresced light at the surface (*FLH*, described further in this section) by the amount of light absorbed by phytoplankton in the upper water column (*ARP*, described further in this section); hence, it is intended to provide an estimate of the quantum yield of fluorescence. This section provides a short description of the methods developed by the MODIS science team to obtain the *CFE*; a complete description is given in MODIS ATBD 19 (Carder et al. 1999*a*), 20 (Carder et al. 2003), and 22 (Abbott and Letelier 1999).

The fluorescence line height (*FLH*, provided in W m^{-2} μm^{-1} sr^{-1} and converted to mol m^{-2} s^{-1} nm^{-1} sr^{-1} for our calculations) is the MODIS measurement of L_f (*see* Eq. 3). The *FLH* is measured by subtracting from radiance at 678 nm the radiance due to backscattered and Raman scattered photons at 678 nm, which is estimated using a linear baseline between 667 nm and 748 nm. The MODIS *FLH* algorithm uses the top of atmosphere upwelling radiance, which is corrected for Rayleigh scattering, but not aerosol scattering, thus assuming that upwelling radiance is a linear function of wavelength for aerosol scattering.

By applying the Beer-Bouguer-Lambert law to photons emitted at depth, we can define a depth, z_{678}, at which the upwelling fluoresced radiance is attenuated by 63.2% at the surface:

$$z_{678} \approx \frac{cos(\theta')}{a_w(678)+a_\varphi(678)}. \quad (5)$$

The amount of visible radiation absorbed by phytoplankton (*ARP*) over that depth is

$$ARP = \int_{400}^{700}\int_0^{z_{678}} a_\varphi(\lambda)\cdot\overset{o}{E}(\lambda,0)\cdot e^{-K(\lambda)\cdot z}\cdot dz\cdot d\lambda =$$
$$\int_{400}^{700} a_\varphi(\lambda)\cdot\overset{o}{E}(\lambda,0)\cdot\left[\frac{1-e^{-K(\lambda)\cdot z_{678}}}{K(\lambda)}\right]\cdot d\lambda \quad (6)$$

where $a_\varphi(\lambda)$ and $K(\lambda)$ are retrieved by a semi-analytical model that also retrieves chlorophyll concentration and gilvin absorption (Carder et al. 1999*a*; Carder et al. 2003) using MODIS measurements of water-leaving radiance in all bands from 412 to 551 nm. Since it uses the band at 412 nm, this algorithm, despite its accuracy in many locations (Carder 2003), may be more affected by a poor atmospheric correction than empirical algorithms using only longer wavelengths: the 412 nm waveband shows the largest errors in retrievals (Gordon 2002) even under ideal conditions. Note that the MODIS ATBD 20 (version 7) describes z_{678} as $z_{685} \approx cos(\theta')/\left[a_w(685)+a_\varphi(675)\right]$. The waveband for water is from an older specification of the MODIS sensor, and the algorithm will be changed to 678 nm (i.e., Eq. 5) to reflect the present specifications (Carder pers. comm. unref.).

The *CFE* is obtained as *CFE* = *FLH/ARP*. To compare with Eq. 4 for φ, this can be written as (using Eq. 6):

$$CFE = FLH\cdot 4\pi\cdot C_f\cdot\left[\int_{400}^{700} a_\varphi(\lambda)\cdot\overset{o}{E}(\lambda,0)\cdot\left[\frac{1-e^{-K(\lambda)\cdot z_{678}}}{K(\lambda)}\right]\cdot d\lambda\right]^{-1} \quad (7)$$

where C_f=43.38 nm for the MODIS bands and was calculated as

$$C_f = \int_{-\infty}^{\infty} f(\lambda)\cdot d\lambda \Big/ \left(f(677) - baseline(677)\right)$$

where $f(\lambda)$ is the fluorescence emission spectrum (assuming a Gaussian distribution with a width at half-maximum of 25 nm centered and normalized to 683nm), $f(677)$ is the same Gaussian evaluated at 677 nm, and baseline (677) is the value of a linear baseline from 665 to 747 nm at 677 nm (Letelier pers. comm. unref.). In practice, a small constant is added to *FLH* before dividing by *ARP* to account for negative values of *FLH* encountered at low chlorophyll concentrations under remote sensing conditions (*see* section: Analysis of MODIS data, and Abbott and Letelier 1999). The use of 677 nm is consistent with the MODIS band for fluorescence emission being centered at 676.7 nm.

Procedures

Analysis of MODIS *data*—MODIS level 3 datasets from reprocessing version 4.0 were obtained from the Goddard Distributed Active Archive Centers (DAAC) for 15 January 2001 (inspection of data from the 4.1 reprocessing shows very little change for the regions and days studied). The dataset comprises three estimates of chlorophyll concentration (case 1 pigment algorithm, case 2 algorithm, and SeaWiFS analog); *CFE*; *ARP*; *FLH*; sea surface tem-

perature; the attenuation coefficient at 490 nm ($K_d(490)$, m^{-1}); an instantaneous estimate of the photosynthetically available radiation (PAR) irradiance at the time of the satellite overpass (based on the model of Gregg and Carder 1990, referred to as ipar) (*see* ATBD 20); and quality flags. We used the SeaWiFS analog chlorophyll algorithm (SeaWiFs algorithm using MODIS bands, switching between reflectance ratios 443/551 and 488/551) to compare our algorithm for chlorophyll from fluorescence with those of MODIS. Two other chlorophyll algorithms are used during a sensitivity analysis of our algorithms. The case 2 algorithm is a semi-analytical inversion algorithm and also retrieves the absorption by gilvin (Carder et al. 1999*b*) while the case 1 water algorithm is an empirical relationship based on high-performance liquid chromatography chlorophyll concentration and a blue-to-green waveband ratio (Clark 1999). The algorithm for the attenuation coefficient at 490 nm is described in Clark (1999) and Mueller (2000). It uses a power function of the ratio of the water leaving radiance at 488 and 551 nm. Larger uncertainties in this algorithm are expected with an increasing attenuation coefficient: from 18% at $K_d(490) < 0.2$ m^{-1} to 50% at $K_d(490) > 0.3$ m^{-1} (Clark 2001). In our algorithms, we used the standard *FLH* product such that a small value, FLH_o, has been added to *FLH* to avoid negative radiances encountered due to the top of the atmosphere (minus Rayleigh scattered radiance) measurement of *FLH*.

Two subscenes were selected for examination: one from the Arabian Sea and one off the west coast of Central America including the Costa Rica Dome. Only pixels that achieved the highest quality level (quality flag = 0) set by the ATBD were included in the analysis.

Note that the ipar product, despite being validated, had some spatial inconsistencies, especially near the sunglint region. The regions chosen for this analysis are relatively far from the main region of sunglint and should not be greatly affected. In any case, this should not influence the comparison of the MODIS *CFE* and our quantum yield as they will both be affected equally. However, the *CFE* or our estimate of the yield may show trends versus ipar or increased variability that are not natural. The ipar algorithm is being corrected by the MODIS science team.

The algorithms

Overview—We will now describe two new fluorescence algorithms for retrieving chlorophyll concentration and the quantum yield. The *FLH* contains information on both the quantum yield of fluorescence and chlorophyll concentration (*see* Eq. 4); however, to obtain information about one requires assumptions about—or measurement of—the other.

In case 1 waters (Morel and Prieur 1977), variability in the optical characteristics of the water column are influenced mostly by the abundance of phytoplankton and associated materials. This characteristic has allowed the development of ocean color algorithms based on phytoplankton biomass (expressed in terms of chlorophyll concentration). In this study, we use the diffuse attenuation coefficient at 490 nm ($K_d(490)$, m^{-1}) instead of chlorophyll to characterize trends of optical properties. Our approach is similar to the one proposed by Babin et al. (1996*b*); however, we depart from their chlorophyll-based calculation, thereby deriving an estimate of *chl* from fluorescence emission that does not require another estimate of *chl* as input. It should be stressed that both the standard chlorophyll algorithms and $K_d(490)$ are obtained using ratios of blue-to-green upwelling radiance. In case 1 waters, phytoplankton absorption and covarying matter are the dominant sources of variability affecting the blue-to-green ratio. Hence, $K_d(490)$, phytoplankton absorption, and chlorophyll concentration are strongly correlated to each other (Morel and Maritorena 2001) in these waters. Our chlorophyll algorithm should be considered an approach using information from both the blue-to-green ratio and fluorescence region to estimate chlorophyll. Furthermore, we consider $K_d(490)$ to be a more direct descriptor of the optical properties of the water column than chlorophyll, as it is directly dependent on the inherent optical properties (Kirk 1994) which themselves, in addition to the angular dependence of the light field, define the water-leaving radiance measured by MODIS (e.g., Morel et al. 2002).

The empirical relationships required between $K_d(490)$ and the optical properties of phytoplankton and the water column are those that will specify a simplified version of Eq. 3 and allow the retrieval of φ and *chl*. Assuming that *FLH* retrieves L_f perfectly we can write:

$$FLH = \frac{chl \cdot Q_a^* \cdot \varphi \cdot \bar{a}_\varphi^* \cdot \overset{o}{E}_{PAR}(0)}{4\pi \cdot C_f} \cdot \left[K_{abs}^{\tau_f} + \frac{a_f}{\cos(\theta')} \right]^{-1} \quad (8)$$

The parameter $K_{abs}^{\tau_f}$ is the attenuation coefficient for downwelling absorbed irradiance, evaluated to depth, z_{90}, above which 90% of the fluorescence radiance at the surface originates, and

$\bar{a}_\varphi^* = \int_{PAR} a_\varphi^*(\lambda) \cdot \overset{o}{E}(\lambda, 0) \cdot d\lambda \Big/ \int_{PAR} \overset{o}{E}(\lambda, 0) \cdot d\lambda$ is the irradiance-weighted chlorophyll specific absorption coefficient (e.g., Morel 1978). In this work, the value of $K_{abs}^{\tau_f}$ satisfies the following equation in a least square sense from $z = 0$ to z_{90}:

$$\ln\left[A_{abs}(z) / A_{abs}(0^-) \right] = -K_{abs}^{\tau_f} \cdot z \Big|_{z=0}^{z_{90}}.$$

The relationships to be specified are Q_a^*, $\bar{a}_\varphi^*$, a_f, and $K_{abs}^{\tau_f}$ as functions of $K_d(490)$ (Fig. 1), and are described in the next sections.

Equation 8 represents almost all of the spectral effects in Eq. 3 in a much simpler form. This is accomplished in two ways. First, $\bar{a}_\varphi^*$ is parameterized as a function of $K_d(490)$ at the surface, thereby accounting for the variability in the phytoplankton absorption spectrum as a function of trophic status (Bricaud et al. 1995; Ciotti et al. 1999; Ciotti et al. 2002). We approximate $\bar{a}_\varphi^*$ as $a_\varphi^*(512)$, which can be done since phytoplankton absorption at 512 nm is nearly equal to $\bar{a}_\varphi^*$ over the photosyntheti-

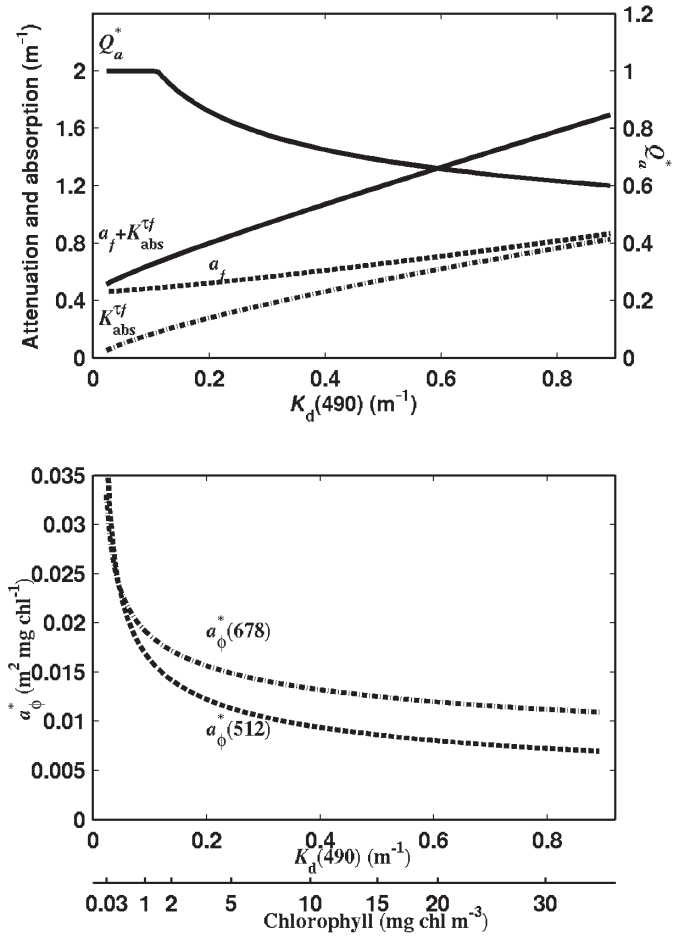

Fig. 1. Relationships between the optical properties of phytoplankton and water. Top: Q_a^*, a_f, and $K_{abs}^{\tau_f}$. Bottom: $a_\varphi^*(512)$ and $a_\varphi^*(678)$. These parameters are applied to the upwelling fluorescence radiance to retrieve chlorophyll and φ in our algorithms; *see* text and Table 1 for description of symbols. The bottom axis shows the chlorophyll concentration for a given K_d (490) from the relationship of Morel and Maritorena (2001).

cally available radiation range (PAR, 400 to 700 nm) for a wide range of phytoplankton absorption spectra (Bricaud et al. 1995; Ciotti et al. 2002) and a typical solar irradiance spectrum at the surface (data not shown). Secondly, the depth dependence of the spectral light field influencing phytoplankton fluorescence is well accounted for by the attenuation coefficient for the absorbed irradiance (see equation 12 and accompanying text).

Deriving Q_a^*, $\overline{a}_\varphi^*$, and a_f as functions of K_d(490)—To derive relationships for Q_a^*, $\overline{a}_\varphi^*$, and a_f, we used the models of (1) Bricaud et al. (1995) relating $a_\varphi^*(\lambda)$ to *chl* and (2) Morel and Maritorena (2001) relating *chl* and $K_d(\lambda)$. We solved for a_φ (678) (m^{-1}), a_φ^*(678) (m^2 mg chl^{-1}), and $\overline{a}_\varphi^*$ (m^2 mg chl^{-1}) as functions of K_d(490):

$$a_\varphi(678)=0.4762\cdot(K_d(490)-0.016)^{1.22} \quad (9)$$

$$a_\varphi^*(678)=0.0106\cdot(K_d(490)-0.016)^{-0.229} \quad (10)$$

$$\overline{a}_\varphi^*=a_\varphi^*(512)=0.00663\cdot\left(K_d(490)-0.016\right)^{-0.3611}. \quad (11)$$

The parameter Q_a^* was obtained from the ratio $a_\varphi^*(678)/a_{sol}^*$ (678) (Morel and Bricaud 1981) where $a_{sol}^*(678)$ = 0.0182 m^2 mg chl^{-1} is the chlorophyll-specific absorption coefficient for chlorophyll in solution (Bidigare et al. 1990). Using this relationship, we find that when $K_d(490) < 0.11$ m^{-1}, $Q_a^* > 1$, which is physically unrealistic. Thus, Q_a^* has been set to 1.0 for $K_d(490) < 0.11$ m^{-1} (see Fig. 1). We used $a_f = a_w(678) + a_\varphi(678)$ where $a_w(678)$ is 0.461 m^{-1} from Pope and Fry (1997).

Babin et al. (1996b, their Eq. 3) described a relationship for $\overline{a}_\varphi^*$, which, when recast in terms of $K_d(490)$, is $\overline{a}_\varphi^* = 0.00605 \cdot (K_d(490)–0.016)^{-0.3727}$. This is less than 10% different from our parameterization of $\overline{a}_\varphi^*$ over chlorophyll concentrations ranging from 0.03 to 30 mg m^{-3}.

Obtaining $K_{abs}^{\tau_f}$—The form of Eq. 8 implies that the depth of integration is to infinity (as in Eq. 3). However, because $K_{abs}^{\tau_f}$ is a broadband attenuation coefficient that must decrease with depth (cf. Kirk 1994) and fluorescence is rapidly attenuated in water, $K_{abs}^{\tau_f}$ has to be calculated near the surface. So, we used $K_{abs}^{\tau_f}$ derived for the region from which 90% of the water-leaving fluorescence originates.

The attenuation coefficient for absorbed irradiance, $K_{abs}^{\tau_f}$, was obtained by an iterative procedure. First, the absorbed radiation by phytoplankton at each wavelength was computed every 0.02 m from the surface to an initial estimate of the depth above which 90% of surface fluorescence originates (z_{90}, m^{-1}) and summed over wavelength. This was done successively for chlorophyll concentrations from 0 to 30 mg chl m^{-3} using the spectral attenuation coefficients computed from Morel and Maritorena (2001), the spectral chlorophyll-specific absorption coefficients of Bricaud et al. (1995), and a subsurface downwelling irradiance spectrum computed using Gregg and Carder's (1990) model for noon at 45°N at the summer solstice. An attenuation coefficient, $\tilde{K}_{abs}^{\tau_f}$, was computed by fitting a linear function to the natural log of the absorbed radiation versus depth. The depth above which 90% of fluorescence originates was then computed as $2.3/\left[\tilde{K}_{abs}^{\tau_f}+a_f\right]$. This was used in place of the initial estimate of z_{90} and the procedure was repeated; the computation converged after 4 iterations, which provided the iterative solution to the attenuation coefficient $\tilde{K}_{abs}^{\tau_f}$. Despite being a broadband attenuation coefficient, numerical values of absorbed irradiance and those computed using $\tilde{K}_{abs}^{\tau_f}$ at all depths between 0 and z_{90} are within 1% for all simulations.

Finally, a fit of $\tilde{K}_{abs}^{\tau_f}$ as a function of K_d(490) was obtained (see Fig. 1 and Fig. 2):

$$K_{abs}^{\tau_f}=-0.00831+0.908\cdot K_d(490)^{0.718}. \quad (12)$$

Errors in this parameterization as a function of K_d(490) relative to the iterative solution are shown in the lower panel of Fig. 2. Note that the small error at low values of K_d(490) in our parameterization is inconsequential to the retrieval of *chl*

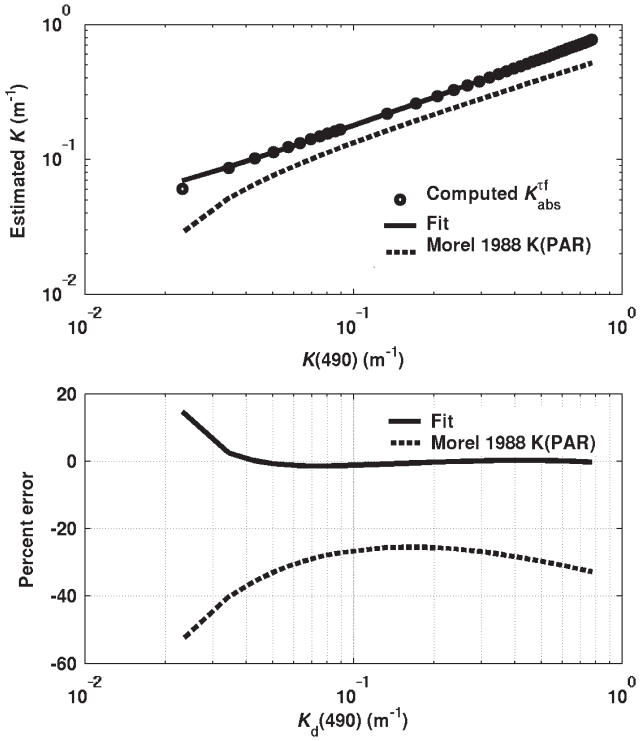

Fig. 2. Attenuation coefficient of fluorescence excitation irradiance. Top panel shows the computed $K_{abs}^{\tau_f}$ using an iterative procedure and the fit to those computations given in Eq. 12, as well as a comparison with the attenuation for PAR irradiance (K(PAR), Morel 1988) for the euphotic zone, expressed as a function of K_d (490), using relationships in Morel and Maritorena (2001). Bottom panel shows the percent error between our parameterization of $K_{abs}^{\tau_f}$ and our iterative computation of $\tilde{K}_{abs}^{\tau_f}$, as well as the percent difference between the parameterization of the fluorescence exciting radiation using K(PAR) and our numerical computations. Errors at low values of K_d(490) are inconsequential for the computation of fluorescence emission at the surface because $K_{abs}^{\tau_f} << a_f$ (*see* Eq. 8).

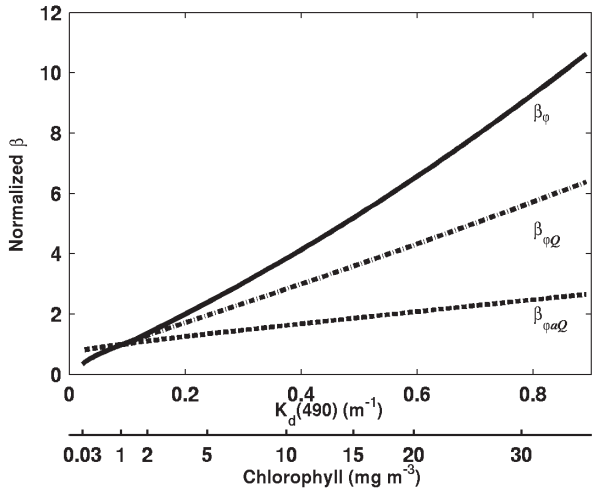

Fig. 3. Correction factors normalized to the value at 1 mg chl m^{-3} applied to *FLH* to retrieve chlorophyll concentration and the quantum yield of fluorescence. These factors were obtained by inserting relationships derived in Eqs. 9 to 12 into Eqs. 13 and 17, respectively (*see* also Fig. 1).

or φ (Eq. 4) since $K_{abs}^{\tau_f}$ is about 10 times lower than a_f in these waters. A comparison is also made with Morel's (1988) parameterization of K(PAR), which shows the error incurred if the attenuation coefficient for PAR integrated over the euphotic zone is used instead of that for the absorbed radiation calculated near the surface. An attenuation coefficient for PAR is sometimes used as an approximation for the excitation radiation (e.g., Babin et al. 1996*b*). For the computation of the quantum yield, this error becomes significant only when K_d(490) is of the same order as a_f (for pure water a_f is ~0.5 m^{-1} in the fluorescence band). When using K(PAR) an underestimate of ~15% will occur in the quantum yield of fluorescence at K_d(490) = 0.5 m^{-1} because a ~30% error in $K_{abs}^{\tau_f}$ with K_d(490) = a_f leads to ~15% error in the quantum yield of fluorescence (Fig. 2).

Quantum yield of fluorescence and chlorophyll concentration—To retrieve the quantum yield of fluorescence and the chlorophyll concentration, the surface fluorescence emission has to be corrected for the bio-optical sources of variability that we have parameterized. Here we apply a factor β_φ that combines terms in the equation for *FLH* (*see* Eq. 8 and Fig. 3):

$$\beta_\varphi = \frac{4\pi \cdot C_f \cdot \left[K_{abs}^{\tau_f} + \left(a_f / cos\,\theta'\right)\right]}{\overline{a}_\varphi^* \cdot Q_a^*}. \qquad (13)$$

Assuming that the statistical model is retrieving the in situ optical properties perfectly, β_φ allows for the retrieval of the two products. First, by replacing the terms on the right-hand side of Eq. 13 with β_φ in Eq. 8 and dividing both sides by φ_{chl}, a constant quantum yield used for estimating chlorophyll concentration, we obtain:

$$FLH \cdot \beta_\varphi / (\varphi_{chl} \cdot \overset{o}{E}_{PAR}) = chl \cdot \varphi / \varphi_{chl}\ . \qquad (14)$$

Assuming a constant ratio of $\varphi/\varphi_{chl} = 1$, our proxy for chlorophyll concentration estimated from fluorescence is

$$chl_{\text{fluo}} = FLH \cdot \beta_\varphi / (\varphi_{chl} \cdot \overset{o}{E}_{PAR}). \qquad (15)$$

For all estimates, we used $\varphi_{chl} = 0.012$. This is the mean quantum yield retrieved by the quantum yield algorithm described below. The MODIS product ipar was used for $\overset{o}{E}_{PAR}$.

Secondly, using β_φ and Eq. 8 as above and the MODIS retrieved chlorophyll (chl_{MODIS}; SeaWiFS analog algorithm), we calculate

$$\varphi_{est} = FLH \cdot \beta_\varphi / (\overset{o}{E}_{PAR} \cdot chl_{\text{MODIS}}). \qquad (16)$$

This is our estimate of the quantum yield.

This approach is based on statistical relationships with K_d(490), which was estimated from the blue-to-green ratio in remotely sensed ocean color. Areas that do not follow the central trends of phytoplankton optical properties with estimates of K_d(490) will show up as variations in the quantum

Table 2. A comparison of the quantum yield parameters

Parameter	Accounts for variability in	Does not account for	Depth of calculation	Estimated variables
CFE	*chl*, $K(\lambda)$, a^*	Q_a^*; Attenuation of incident light when calculating depth of integration	Depth from which 63.2% of the emitted fluorescence is attenuated at the surface	$\varphi \cdot Q_a^*$
φ_{est}	*chl*, $K(\lambda)$, a^*, Q_a^*		Infinity	φ
φ_Q	*chl*, $K(\lambda)$, a^*	Q_a^*	Infinity	$\frac{\varphi \cdot Q_a^*}{\tilde{Q}_a^*}$
φ_{aQ}	*chl*, $K(\lambda)$	a^*, Q_a^*	Infinity	$\frac{\varphi \cdot \bar{a}_\varphi^* \cdot Q_a^*}{\left[\tilde{\bar{a}}_\varphi^* \cdot \tilde{Q}_a^*\right]}$

yield (e.g., the presence of high $\bar{a}_\varphi^*$ at high $K_d(490)$ will show up as a spuriously high quantum yield). Note that changes in β_φ with chlorophyll concentration between 0.03 and 1 mg chl m^{-3} are mostly due to the decrease in $\bar{a}_\varphi^* \cdot Q_a^*$ (see Fig. 1). Furthermore, the parameterizations for $\bar{a}_\varphi^*$ and Q_a^* are only valid for chlorophyll concentrations greater than 0.03 mg chl m^{-3}, and this is also the lower limit of the algorithms developed here.

Our decision to depart from the MODIS ARP algorithm, which is based on the retrieval of phytoplankton absorption, and to use an empirical method based on $K_d(490)$ and empirical chlorophyll estimates was made for several reasons: first, to provide an estimate of the quantum yield independent of the MODIS CFE algorithm (the algorithms are different but the inputs, apart from the 412 nm channel, are the same); second, to make use of the robustness of the empirical chlorophyll algorithms (O'Reilly et al. 1998); and last, to avoid the possible interference of a poor estimate of the 412 nm radiance, which can affect ARP.

Deriving less specific quantum yields—To examine bio-optical sources of variation in the relationship between emitted fluorescence and *FLH*, two parameters were created:

$$\begin{aligned}\beta_{\varphi Q} &= 4\pi \cdot C_f \cdot \left[K_{abs}^{\tau} + \left(a_f / cos\,\theta'\right)\right] \cdot \left[\bar{a}_\varphi^* \cdot \tilde{Q}_a^*\right]^{-1} \\ \beta_{\varphi aQ} &= 4\pi \cdot C_f \cdot \left[K_{abs}^{\tau} + \left(a_f / cos\,\theta'\right)\right] \cdot \left[\tilde{\bar{a}}_\varphi^* \cdot \tilde{Q}_a^*\right]^{-1}\end{aligned} \quad (17)$$

where the tilde signifies that the parameter is held constant at the parameterized value for a chlorophyll concentration of 1 mg m^{-3} ($K_d(490)$ = 0.089 m^{-1}). Further insight can be obtained by following the same approach as above to obtain φ_{est} (Eq. 16), but using $\beta_{\varphi Q}$ and $\beta_{\varphi aQ}$. Using $\beta_{\varphi Q}$ we retrieve φ_Q, which can be interpreted as the quantum yield times a relative fraction of light not reabsorbed within the cell:

$$\varphi_Q = \varphi \cdot Q_a^* / \tilde{Q}_a^*. \quad (18)$$

Using the parameter $\beta_{\varphi Q}$ broadens this mixed physiological index by providing an estimate of the quantum yield divided by a relative index of pigment packaging, φ_{aQ}:

$$\varphi_{aQ} = \varphi \cdot \bar{a}_\varphi^* \cdot Q_a^* \cdot \left[\tilde{\bar{a}}_\varphi^* \cdot \tilde{Q}_a^*\right]^{-1}. \quad (19)$$

It is an index of pigment packaging because both $\bar{a}_\varphi^*$ and Q_a^* decrease as the cell size and pigment packaging increase (Morel and Bricaud 1981). This number is informative as it includes, in one parameter, all the species-dependent and physiologically dependent optical influences on fluorescence.

The subscripts for φ_Q and φ_{aQ} indicate the sources of variability present in these parameters in addition to the quantum yield: i.e., *a* stands for $\bar{a}_\varphi^*$ and *Q* stands for Q_a^*. The φ_Q parameter should be the most similar to CFE because, as with the MODIS product, it does not account for the effect of Q_a^* (*see* Table 2) in the algorithm, hence, any natural variability in this factor will be included in the retrieved product (*CFE* or φ_Q). Note that φ_Q and φ_{aQ} use fewer statistical bio-optical relationships for their retrieval than φ_{est}, so they should be the most accurately derived; however, they are more difficult to interpret than φ_{est}.

Assessment

Relationship between FLH and chlorophyll—Equation 15 can be rewritten as

$$FLH = chl_{\text{fluo}} \cdot \varphi_{chl} \cdot \overset{o}{E}_{PAR} \Big/ \beta_\varphi. \quad (20)$$

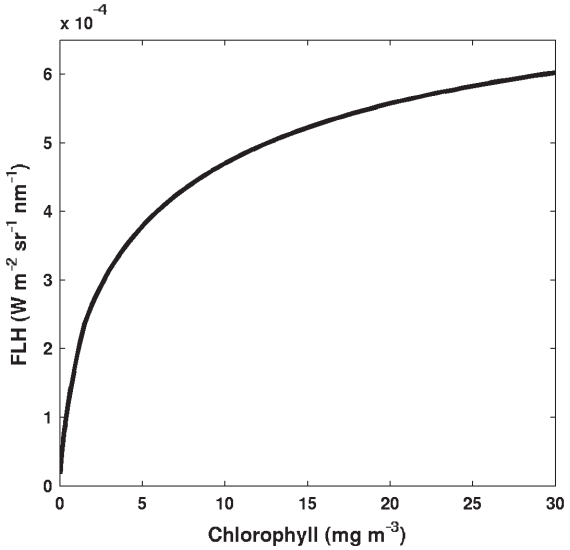

Fig. 4. Relationship between the *FLH* and chlorophyll concentration with our parameterization (*see* Eq. 20) using φ_{chl} = 0.012 and $\overset{o}{E}_{PAR}$ = 1750 µmol m^{-2} s^{-1}.

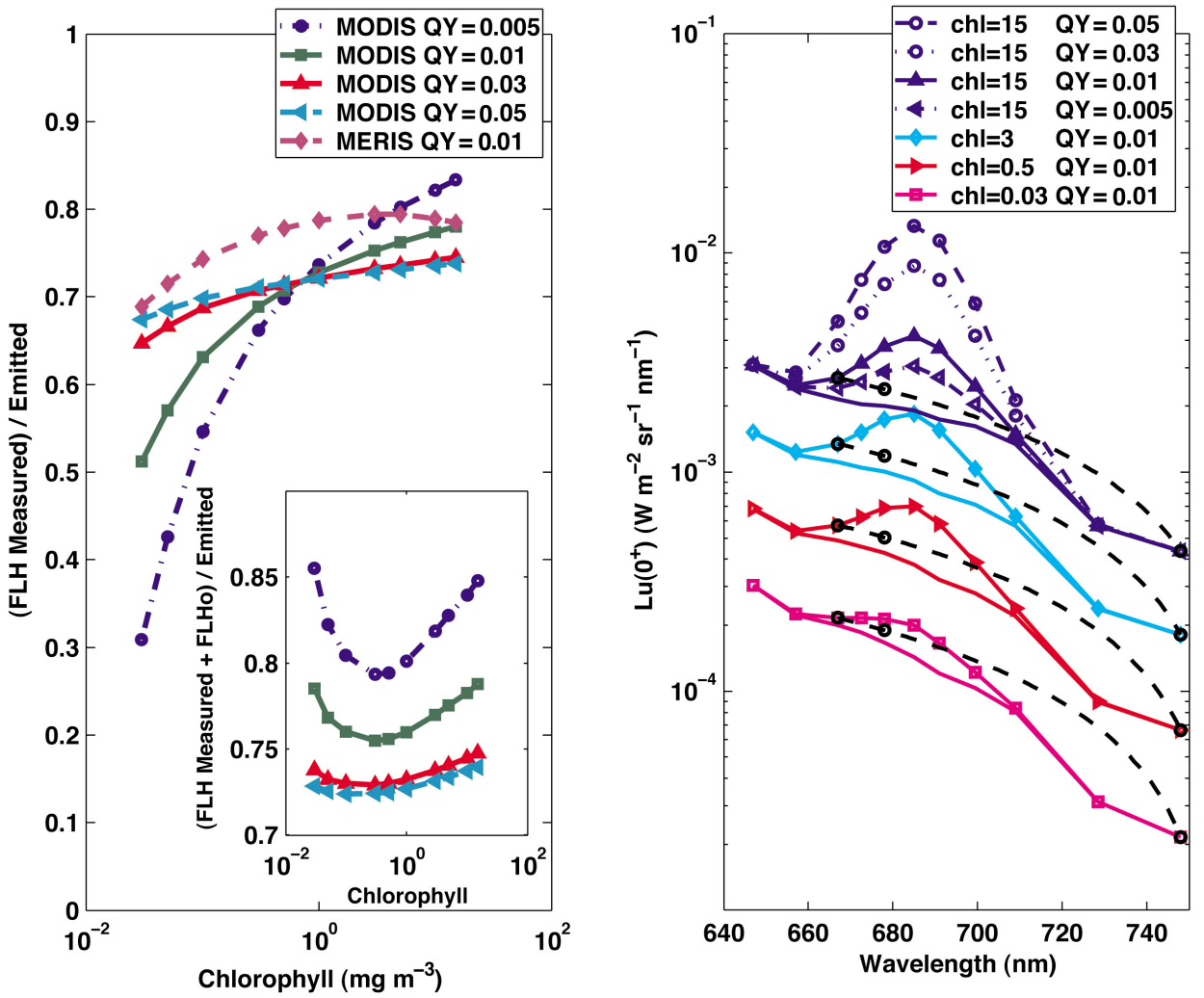

Fig. 5. Modeled relationships between the estimates obtained using the baseline method and emitted fluorescence at 678 nm. The left panel: Ratio of the baseline-measured radiance (equivalent to the *FLH* measurement) to the emitted radiance using Hydrolight simulations of case 1 waters. The emitted radiance was calculated by subtracting the Hydrolight simulation of upwelling radiance just above the surface without fluorescence from the one with fluorescence. Ratios are presented for four baselines using the 667 to 748 nm baseline (identified as MODIS) using quantum yields of 0.005, 0.01, 0.03, and 0.05, and one baseline (MERIS QY = 0.01) using 667 to 709 nm, which is similar to MERIS (which uses 665 to 709 nm) with a quantum yield of 0.01. The inset shows the MODIS simulations with a small baseline value, FLH_o of 1.26×10^{-5} W m^{-2} nm^{-1} sr^{-1} added. Right panel: Representative spectra of upwelling radiance for four chlorophyll concentrations. The colored continuous lines with filled symbols are the simulations with fluorescence (quantum yield = 0.01), the colored lines without symbols are the simulations without fluorescence, and the black line represents the MODIS baseline without the MODIS FLH_o value added. The logarithmic scaling represents the linear baseline as a curve. Symbols represent the wavebands simulated in Hydrolight. For a chlorophyll concentration of 15 mg m^{-3}, a comparison with three other quantum yields is given (*see* legend). The differences between the top colored line and black line for each chlorophyll concentration are equivalent to measured *FLH*, whereas the differences between the line with fluorescence and without fluorescence at 678 represent the emitted fluorescence.

This provides a predictive relationship for the fluorescence line height under the conditions of observation encountered by MODIS (high irradiance near the surface at midday measured using a baseline method at 678 nm). This relationship is shown in Fig. 4 and is similar to relationships derived by Babin et al. (1996*b*) and Gower et al. (2004, *see* their Fig. 2).

Baseline correction—The *FLH* distinguishes photons emitted by chlorophyll fluorescence from the Raman and inelastically scattered photons using a "baseline method." Because our algorithm is based on the *FLH*, we wanted to know if it was an accurate estimate of the fluorescence emitted at the surface of the ocean. We used Hydrolight simulations (*see* Web Appendix 1) to examine the MODIS baseline as well as, with lesser emphasis, the baseline used by the Medium Resolution Imaging Spectrometer (MERIS, the European Space Agency's ocean color sensor). The two baselines underestimated the amount of fluoresced radiance (Fig. 5). Clearly, in the case of the MODIS baseline, the underestimate is strongly a function of the chlorophyll concentration, especially

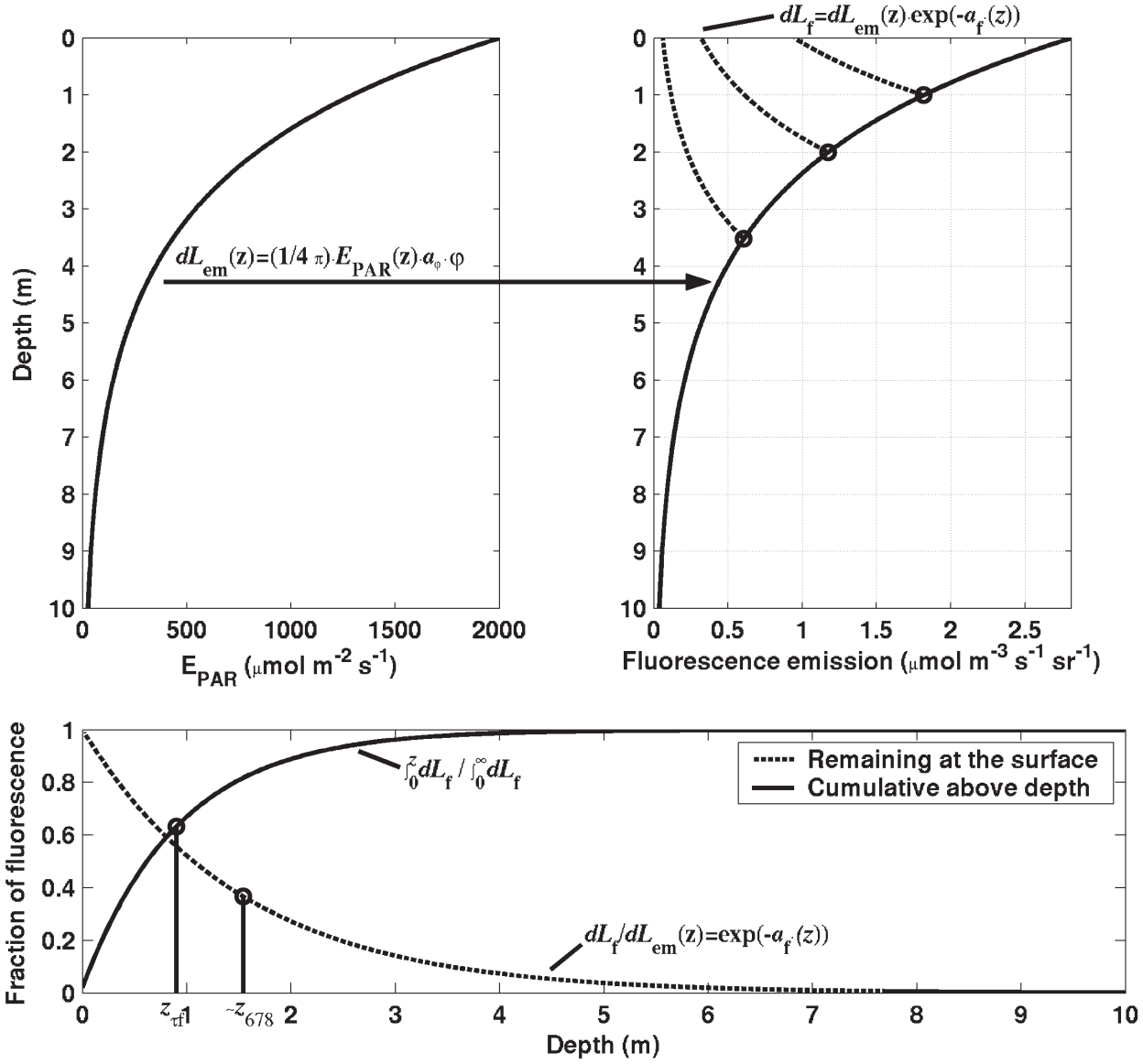

Fig. 6. Simplified model (reduced spectral dependence) of fluorescence emission in water to illustrate the different approaches to calculate the depth where 63.2% of the fluorescence originates. Top left: The incident irradiance in the PAR domain decreases exponentially with depth. Top right: With this simplified model (*see* equation top left), it leads to a decreasing exponential for the volume emission of fluorescence $dL_{em}(z)$ (continuous line). The dashed lines illustrate the decrease in the fluorescence originating from three depths to the surface as it travels up in the water column. The equation above the graph represents the fluorescence just below the surface due to the emission at depth *z*. Bottom panel: The continuous line represents the cumulative emission (as a fraction of the total) at the surface originating from increasingly greater depth intervals. When this cumulative emission reaches 0.632, it corresponds to $z_{\varphi f}$: the depth above which 63.2% of the fluorescence originates. The dashed line represents the volume emission of fluorescence originating from depth *z* remaining at the surface. At a value of 0.378, this corresponds to the depth from which the emitted fluorescence is attenuated by 63.2% at the surface: z_{678}. The depth z_{678} is deeper than $z_{\varphi f}$, which leads to an overestimate of the absorbed irradiance for fluorescence emission. To emphasize the difference, the model presented is consistent with a chlorophyll concentration of 20 mg m^{-3}.

at lower quantum yields. We conclude (*see* web Appendix I for more discussion) that (1) at the sea surface, the baseline corrected fluorescence is not an unbiased measure of the fluorescence emission. The fraction of the total fluorescence emission measured by a baseline corrected spectrum varies with chlorophyll concentration. (2) Given the potential underestimation of fluorescence radiance by *FLH* in low chlorophyll waters, it is expected that a quantum yield algorithm based on *FLH* will return underestimated values in low chlorophyll regions. (3) The addition of a small amount of fluorescence radiance (FLH_o) reduces much of the bias observed with chlorophyll concentration.

Algorithms that do not rely on a baseline estimate for fluorescence emission have been proposed and implemented (Roesler and Perry 1995; Culver and Perry 1997; Coleman et al.

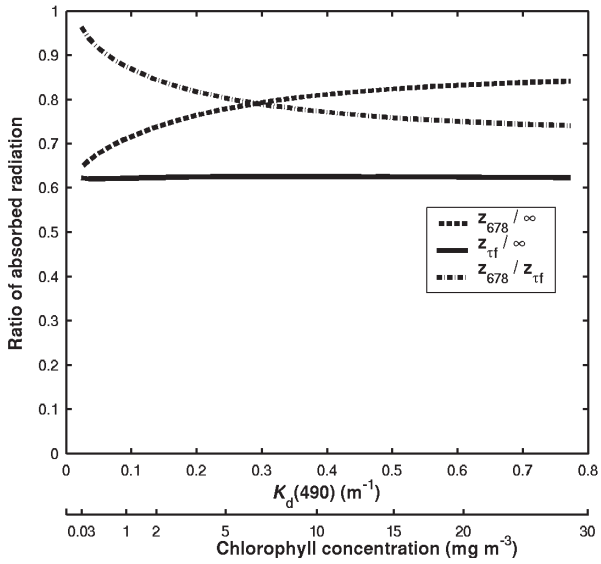

Fig. 7. Ratio of calculated absorbed irradiance weighted for its efficiency of emission at the surface: ($= \int_{400}^{700}\int_{0}^{Z} a_\varphi(\lambda)\cdot \mathring{E}(\lambda,0)\cdot e^{-(K(\lambda)+a_f)\cdot z}\cdot dz\cdot d\lambda$) for different depths Z (see upper bound of second integral above) and a range of chlorophyll concentrations. Our algorithm uses $Z = \infty$. The present MODIS algorithm (*ARP*), which does not account completely for changes in the attenuation of downwelling irradiance, uses $Z = z_{678}$ (Eq. 5). An alternate formulation that accounts completely for the attenuation of downwelling irradiance uses $Z = z_{\tau f}$ (Eq. 21). The ratio of the absorbed weighted irradiance for $Z = z_{\tau f}$, and $Z = \infty$ is equal to 0.632 for all chlorophyll concentrations showing no biases with changes in the attenuation coefficient (line $Z_{\tau f} / \infty$). In high chlorophyll waters, the attenuation of incident light by phytoplankton limits the penetration of light and restricts most of the emission of fluorescence to a layer nearer to the surface than is calculated by the MODIS algorithm, leading to a bias in absorbed radiation calculated using $Z = z_{678}$ compared to $Z = \infty$ (line Z_{678} / ∞). Consequently, the MODIS estimate of *ARP* is high, and estimates of fluorescence efficiency are low. This underestimate varies between ~3% to ~26% as shown by the ratio for $Z = z_{678}$ and $Z = z_{\tau f}$ (line $z_{678}/z_{\tau f}$). The numerical calculations are based on Eq. 3 and the models of Morel and Maritorena (2001) and Bricaud et al. (1995) for nadir observation.

2000; Morrison 2003). Such algorithms may provide a useful method for correcting the fluorescence emission for the backscattered radiance from a remote sensing perspective and could eventually be incorporated into the semi-analytical algorithm presently used to retrieve chlorophyll concentration from MODIS data (Carder et al. 1999*a*; Carder et al. 1999*b*).

Comparing the finite-depth MODIS algorithm to a complete depth model—Other than Q_a^*, which is related to the package effect and is difficult to quantify, the MODIS equation for *CFE* (Eq. 7) differs from Eq. 4 when solved for φ, by the maximum depth of integration representing the source of fluorescence leaving the surface. The MODIS equation integrates to the depth from which the emitted fluorescence is attenuated by 63.2% when it reaches the surface (z_{678}, m; Eq. 5), whereas Eq. 4 integrates to infinity. Since the *ARP* algorithm is intended to account only for absorbed radiation responsible for 63.2% of the surface fluorescence, using *FLH* and *ARP* directly to derive the quantum yield of fluorescence would lead to an overestimate of the quantum yield by approximately 1/0.632, such that a correction has to be applied (Carder et al. 2003).

Rather than integrating to the depth from which the fluorescence emission has been attenuated to 63.2% upon reaching the surface, a more useful depth for interpreting the fluorescence measurement is the depth above which an arbitrary fraction (it could be 63.2%) of the surface-leaving fluorescence originates $z_{\tau f}$ (m) (*see* Fig. 6). It can be obtained by integrating to the depth $z_{\tau f}$ that yields 63.2% of surface leaving fluorescence, integrated to infinity (Babin et al. 1996*b*):

$$\int_{400}^{700}\int_{0}^{z_{\tau f}} a_\varphi(\lambda)\cdot \mathring{E}(\lambda,0)\cdot e^{-(K(\lambda)+a_f)\cdot z}\mathrm{d}z\cdot \mathrm{d}\lambda = 0.632\cdot \int_{400}^{700}\int_{0}^{\infty} a_\varphi(\lambda)\cdot \mathring{E}(\lambda,0)\cdot e^{-(K(\lambda)+a_f)\cdot z}\mathrm{d}z\cdot \mathrm{d}\lambda \quad . \quad (21)$$

This cannot be solved analytically for $z_{\tau f}$ for all wavelengths, but for one excitation wavelength, the solution is $z_{\tau f}(\lambda) = 1/\left(K(\lambda)+a_f\right)$. Therefore, the depth above which 63.2% of surface fluorescence originates depends not only on the attenuation of emitted radiation a_f, but also on the attenuation of the incident irradiance, $K(\lambda)$. This has been omitted in the MODIS estimation of z_{678} (Eq. 5) and should lead to an overestimate of *ARP* and an underestimate of the *CFE* when the approximation $a_f >> K$ does not hold, for example, when the concentration of chlorophyll is high (*see* Fig. 7). Variable attenuation of absorbed radiation does have a strong influence on spatial patterns in some regions (*see* for example Fig. 8 and Fig. 12) and should be accounted for. This is particularly important when interpreting spatial changes in the quantum yield across gradients of chlorophyll.

Although integrating to $z_{\tau f}$ instead of z_{678} provides an unbiased measure of surface absorption, we do not see any advantage gained by limiting the calculation of the absorbed radiation to a restricted depth range since (1) the satellite measures fluorescence that comes from all depths. (2) It is impossible to separate fluorescence from top layers of the water column from that originating deeper. (3) The quantum yield and the chlorophyll concentration vary with depth, hence a given depth will not provide a given fraction of the fluoresced radiance.

We therefore suggest integrating over the whole water column when calculating absorbed radiation for the interpretation of remotely sensed fluorescence. While integration to infinity does not overcome the problems associated with the third point (which is probably small due to the natural weighting to surface depths for the natural fluorescence emission), it removes the false impression that a narrow depth of integration provides results that are less affected by depth variations in optical and physiological parameters.

Comparison of the algorithms: Chlorophyll—The MODIS estimates are shown in Fig. 8 for the subscene off the west coast of Central America. The jet of high chlorophyll concentration observed off the coast of Costa Rica is a persistent phytoplank-

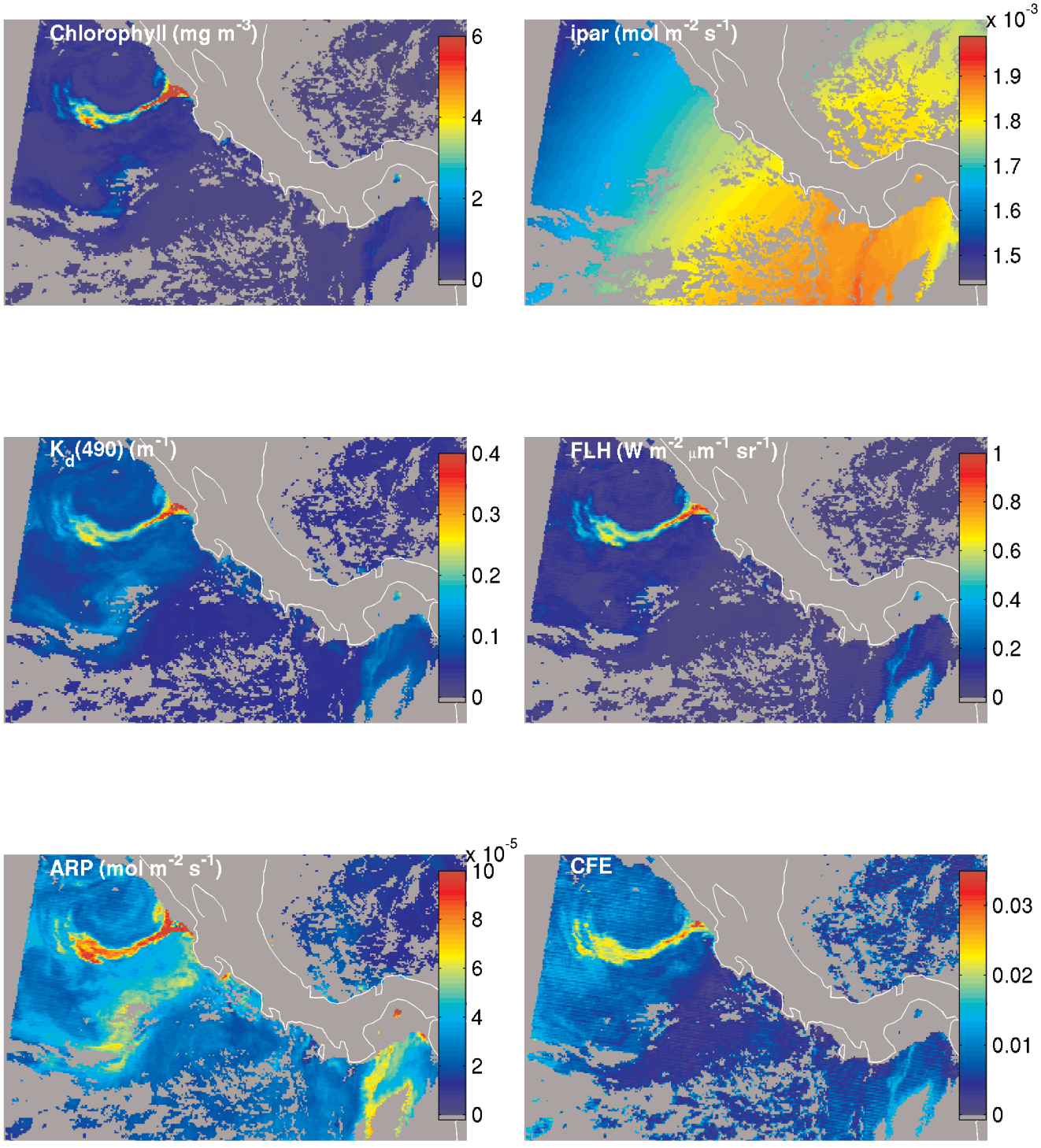

Fig. 8. MODIS level 3 dataset for 15 Jan 2001 for the subscene off the west coast of Central America. The chlorophyll concentration is from the MODIS SeaWiFS analog algorithm, K_d (490) is derived empirically from band ratios, ipar is MODIS model output for clear sky conditions of the instantaneous PAR radiation at the time of the image, *ARP* is the absorbed radiation by phytoplankton, *FLH* is the fluorescence line height (a measure of the amount of fluoresced radiance at the surface of the ocean), and *CFE* is the MODIS estimate of the quantum yield of fluorescence.

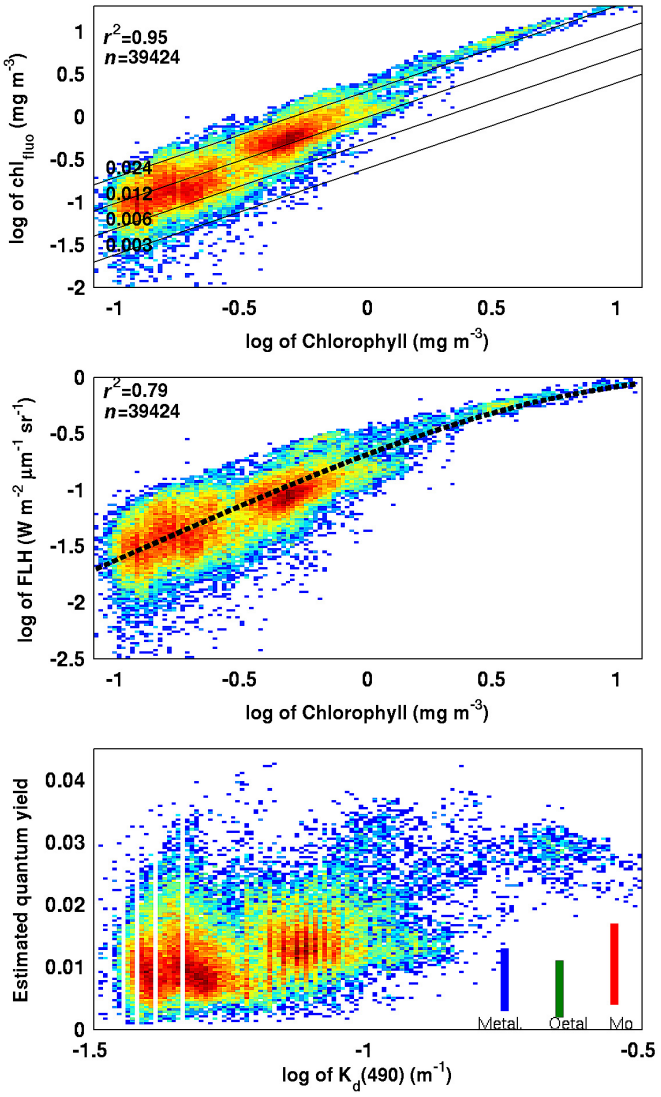

Fig. 9. Top panel: Comparison of our fluorescence estimate of the chlorophyll concentration, $chl_{\text{fluo}} = FLH \cdot \beta_{\varphi} / (\varphi_{chl} \cdot E_{PAR})$ (*see* Eqs. 8 and 14) with MODIS chlorophyll product (chlor_a2, SeaWiFS analog chlorophyll algorithm). The lines are isolines of retrieved quantum yields as indicated, and the line 0.012 is equivalent to a 1:1 correspondence of chl_{fluo} and chl_{MODIS}. The middle panel is the comparison between *FLH* and chlorophyll concentration from MODIS. The dashed black line is the relationship derived by Gower et al. (2004). $FLH = 0.15 \cdot chl/(1+0.2 \cdot chl)$ multiplied by 1.65 to fit the data. Note that the *FLH* was not converted to quantum units for this comparison. Bottom: retrieved quantum yield of fluorescence, φ_{est}, as a function of K_d (490). The colored bars indicate a range of quantum yields measured at the surface of the ocean in situ: "Metal" = Maritorena et al. (2000), "Oetal" = Ostrowska et al. (1997) data for $E_{PAR} > 1 \times 10^{20}$ quanta m^{-2} s^{-1}, and "Mo" = Morrison (2003).

ton bloom extending from the Costa Rica coast into the Costa Rica Dome due to wind-driven upwelling (Fiedler 2002; McClain et al. 2002). Note the close correspondence between chlorophyll, K_d(490), and *FLH*: the first two parameters are derived from similar band ratios while the third is independent of ratios. The jet off the coast of Costa Rica also shows higher *CFE*.

The coefficient of determination for the untransformed values between the chlorophyll retrieved using the fluorescence algorithm developed here and the MODIS retrieved chlorophyll using the SeaWiFS analog algorithm (top panel Fig. 9) is $r^2 = 0.95$ ($n = 39424$), but the slope does not correspond to a constant quantum yield. The diagonal lines in the top panel are isolines of our retrieved quantum yield. The line labeled 0.012, the assumed φ_{chl} for retrieving chlorophyll, is equivalent to a 1:1 line for chl_{fluo} versus chl_{MODIS}. It is clear that the variability in the MODIS chlorophyll concentration explained by the fluorescence chlorophyll algorithm is lower at lower chlorophyll concentrations.

Comparison between *FLH* and the MODIS estimate of chlorophyll shows a clear curvature due to changes in optical properties with increasing chlorophyll concentration and a lower r^2 (0.79, $n = 39424$, middle Fig. 9). We also show a comparison with the model of Gower et al. (2004), which is based on average values of measured fluorescence emission scaled to irradiance for the sun at zenith (middle Fig. 9, dashed black line). Their model follows the central trends of the MODIS data in this region. Part of the variability in the top and middle panels is due to variability in the quantum yield of fluorescence, the chlorophyll-specific absorption coefficient, the error in the determination of chlorophyll from band ratios, and the striping due to detector-to-detector calibration observed in MODIS images (Gower et al. 2004; Salomonson 2004). It should also be kept in mind that the depths sampled by the ocean color and fluorescence techniques are different and become more similar as chlorophyll concentration increases. Despite these errors, for this region, the chlorophyll concentration retrieved using fluorescence is, in most cases, within a factor of 2 of the MODIS estimates of chlorophyll from ocean color; 86% of the points fall within a retrieved yield of 0.006 and 0.024 while 1:1 is 0.012 (top Fig. 9). In addition, the variability in the retrieval of chlorophyll from fluorescence seems to be reduced at higher chlorophyll concentrations (*see* Fig. 9).

Comparison of the algorithms: Sources of variability—A map of chl_{fluo}, calculated assuming a constant φ_{chl} of 0.012, is presented in the upper left panel of Fig. 10. It can be compared with the chlorophyll map in Fig. 8. Our estimate of φ_{est}, using chl_{MODIS} (Eq. 16), is shown in the bottom left panel of Fig. 10. Comparison with MODIS *CFE* (Fig. 8) shows essentially the same features, and the interpretation of spatial patterns in either map would be the same. The parameters φ_Q and φ_{aQ} retrieved using $\beta_{\varphi Q}$ and $\beta_{\varphi aQ}$, respectively, are shown in the upper and lower right panels of Fig. 10. Note the almost complete disappearance of the plume in φ_{aQ}, while φ_Q has an intermediate pattern between φ_{aQ} and φ_{est}, showing that the packaging of pigments modeled as a function of K_d (490) has a strong influence on the retrieval of the quantum yield, the effect of $\bar{a}_{\varphi}^{*}$ being the most important.

Comparison of the algorithms: quantum yield—The magnitude of the retrieval of φ_{est} compares well (Fig. 9, bottom) with the

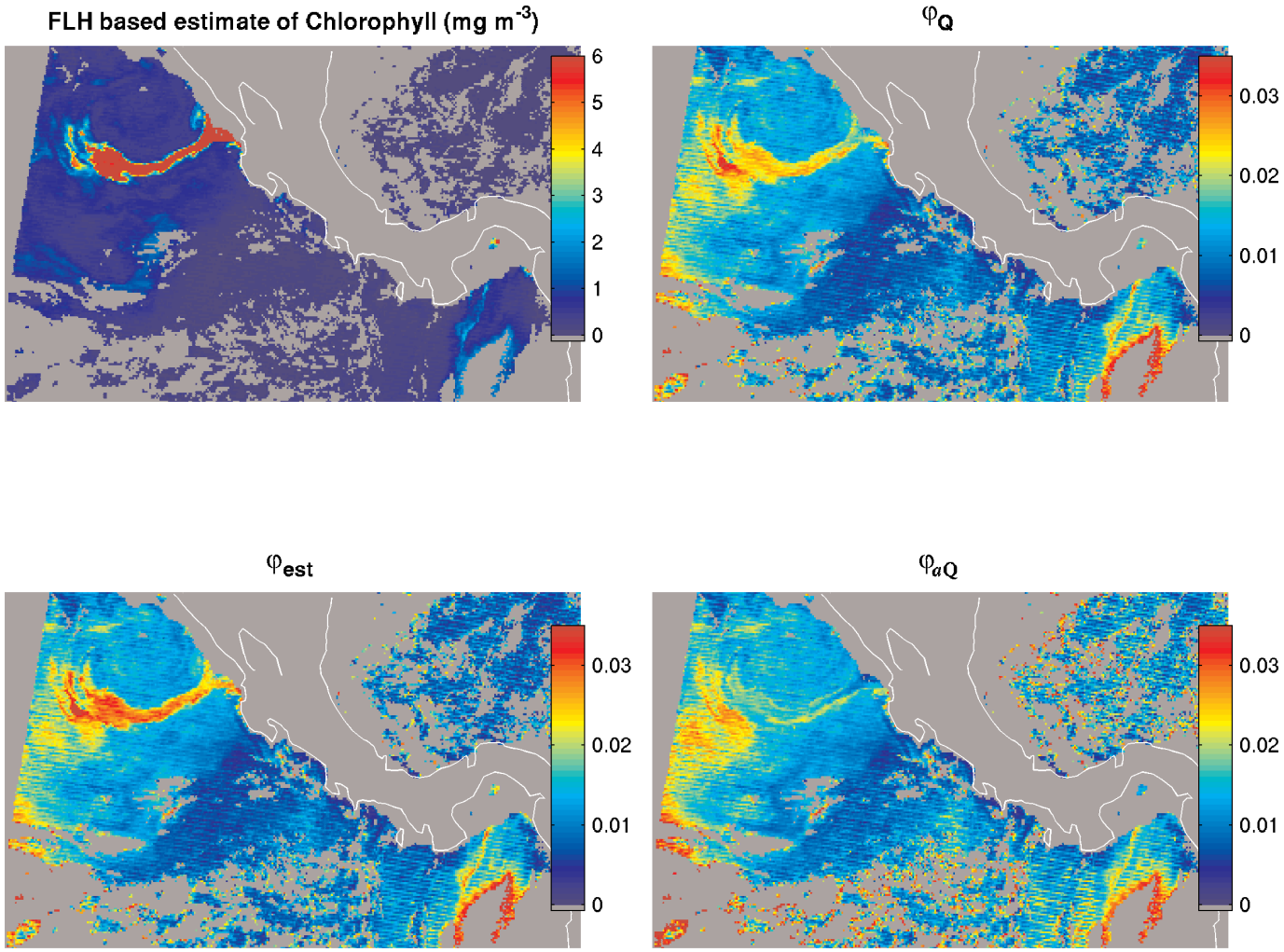

Fig. 10. Map of derived products. Upper left panel is a fluorescence-based estimate of chlorophyll assuming a fluorescence quantum yield (φ_{chl}) of 0.012: $chl_{\text{fluo}} = FLH \cdot \beta_{\varphi}/(\varphi_{chl} \cdot E_{PAR})$. The bottom left shows the estimate of the quantum yield using chlorophyll concentration estimated from blue to green radiance ratios (chl_{MODIS}): $\varphi_{est} = FLH \cdot \beta_{\varphi}/(E_{PAR} \cdot chl_{\text{MODIS}})$. Right panels are the same as bottom left except using corrections $\beta_{\varphi Q}$ (upper) and $\beta_{\varphi \alpha Q}$ (lower) instead of β_{φ}.

yields measured in situ in surface waters of the world (Ostrowska et al. 1997; Maritorena et al. 2000; Morrison 2003). A comparison of φ_{est} and *CFE* is shown in the upper left panel of Fig. 11. To explore bias in the two yields relative to each other, the ratio of φ_{est} /*CFE* is plotted as a function of (1) $K_d(490)$ (upper right), (2) absorption by gilvin, which includes chromophoric dissolved organic matter and non-living particulate matter, at 400 nm (lower left), and (3) *ARP* (lower right). Absorption by gilvin is a standard MODIS product obtained from the same semi-analytical inversion algorithm that returns an estimate of chlorophyll concentration (the case 2 waters algorithm). Very little bias was observed in this region except for a lower ratio at high values of $K_d(490)$ and absorption by gilvin. The comparisons for this region (Fig. 11) show that the CFE and our algorithm for the quantum yield provide similar results, but *CFE* is lower by a factor of 0.58. The cause of this systematic difference is unknown, but could originate in part from our use of Q_a^*. It is, however, in the opposite direction from the bias that would be incurred if the correction for the overestimate of *CFE* by 1/0.632 due to the shallow depth measurement had not been applied (*see* equation 21 and accompaning text).

Comparison of the algorithms: Arabian Sea—The MODIS measurements for the Arabian Sea (Fig. 12) show patterns consistent with hydrographic forcing, with the possible exception of the *ARP* and *CFE* maps, which show a strong feature (high *CFE* and low *ARP*) going across the image in a northeast-southwest direction that is not present in the other maps. The relationship between the MODIS estimates of chlorophyll and fluorescence-based estimates is more variable in this region (Fig. 13, top and middle). There is a clear offset showing lower chl_{fluo} at values of

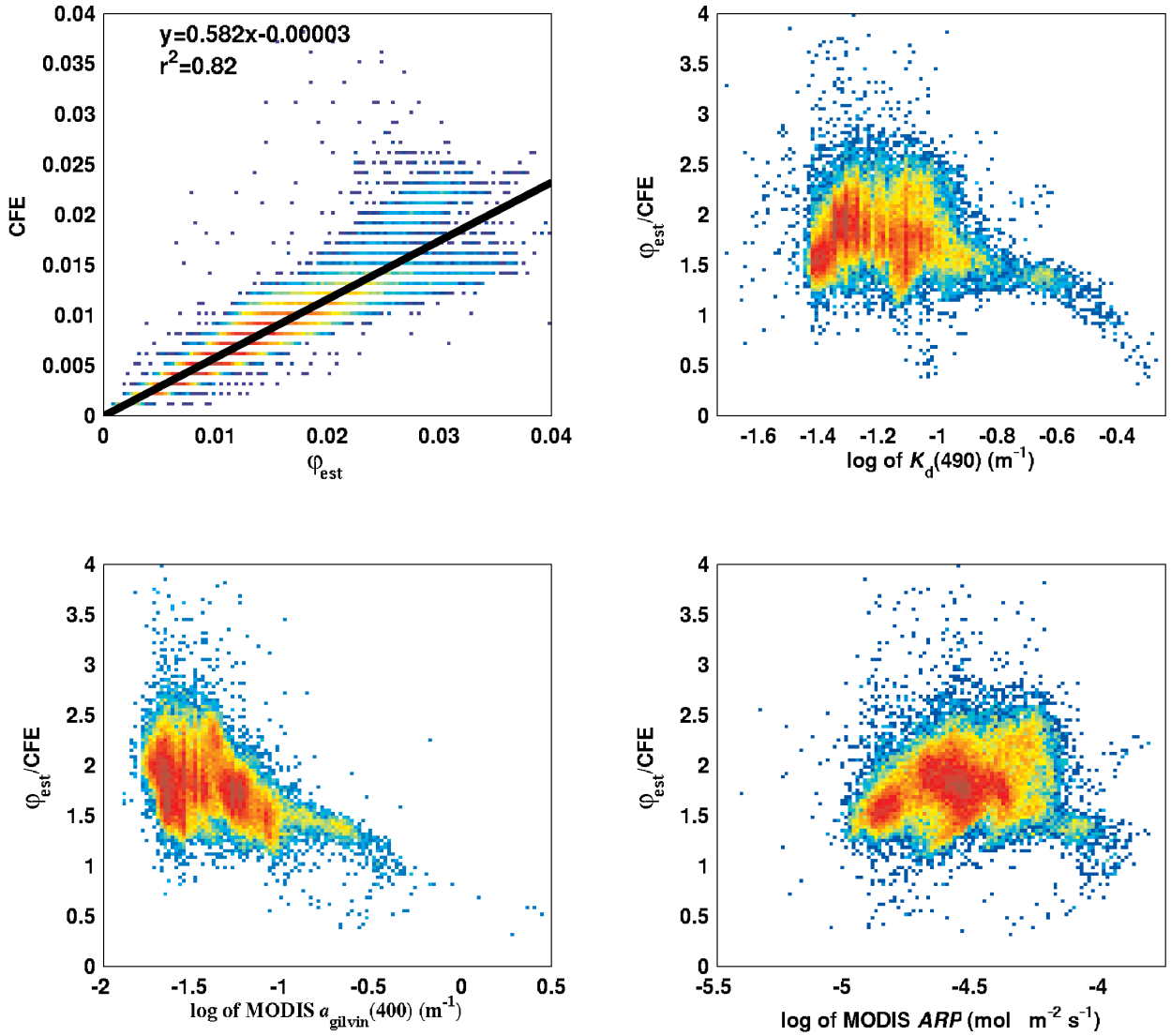

Fig. 11. Comparison of quantum yields. Upper panel compares the quantum yield estimated from our method (φ_{est}) and the MODIS estimate (*CFE*), the line is the best fit to the data. The remaining panels show the ratio of φ_{est} to *CFE* as a function of K_d (490) (upper right), absorption by gilvin at 400 nm (lower left), and *ARP* (lower right).

MODIS chlorophyll ~1 to 3 mg m^{-3}, which corresponds mostly with coastal waters. The central trends are, however, the same as for the previous region. The Gower et al. (2004) algorithm (using the same scaling as in Fig. 9) underestimates the chlorophyll concentration. Note that Gower and colleagues suggest that the chlorophyll-specific surface fluorescence emission should vary depending on the solar zenith angle. However, they did not describe the mathematical relationship. So we kept the same scaling as in Fig. 9 because it provides a good reference for comparison. Because the median of our retrieved φ_{est} was the same as for the previous region (~0.012), the difference is probably due to overall lower ipar values in this region and not a change in the quantum yield. The decreased variability explained in MODIS estimates of chlorophyll by chl_{fluo} (Fig. 9 vs. Fig. 13) may, in part, be due to larger error in the MODIS chlorophyll algorithm, since this region seems more optically complex, as highlighted by the apparent artifact in the *CFE* and *ARP* algorithms, which lead to a stripe going across the image.

The patterns of retrieved quantum yield versus K_d(490) (Fig. 13, bottom) are different from those observed in Fig. 9 especially at high K_d(490). Whereas in Fig. 9 the high values of K_d(490) were associated with the upwelling plume, in Fig. 13 the high values are located near the coast and are probably influenced by river runoff.

A comparison of the maps of φ_{est} (Fig. 14) and *CFE* (Fig. 12) shows striking differences: the stripe showing high values of *CFE*

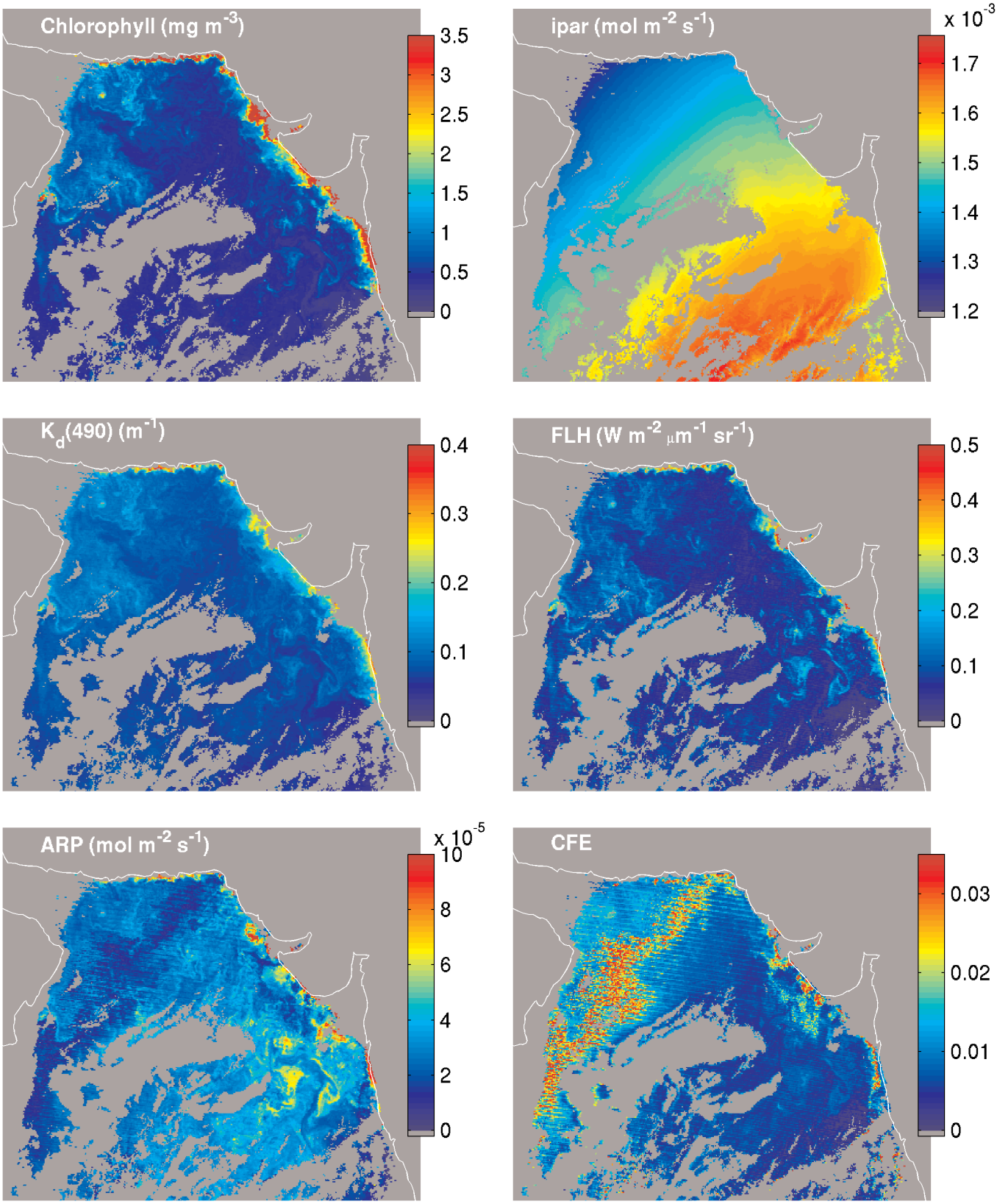

Fig. 12. MODIS level 3 dataset for 15 Jan 2001 for the subscene of the Arabian Sea. *See* Fig. 8 for details.

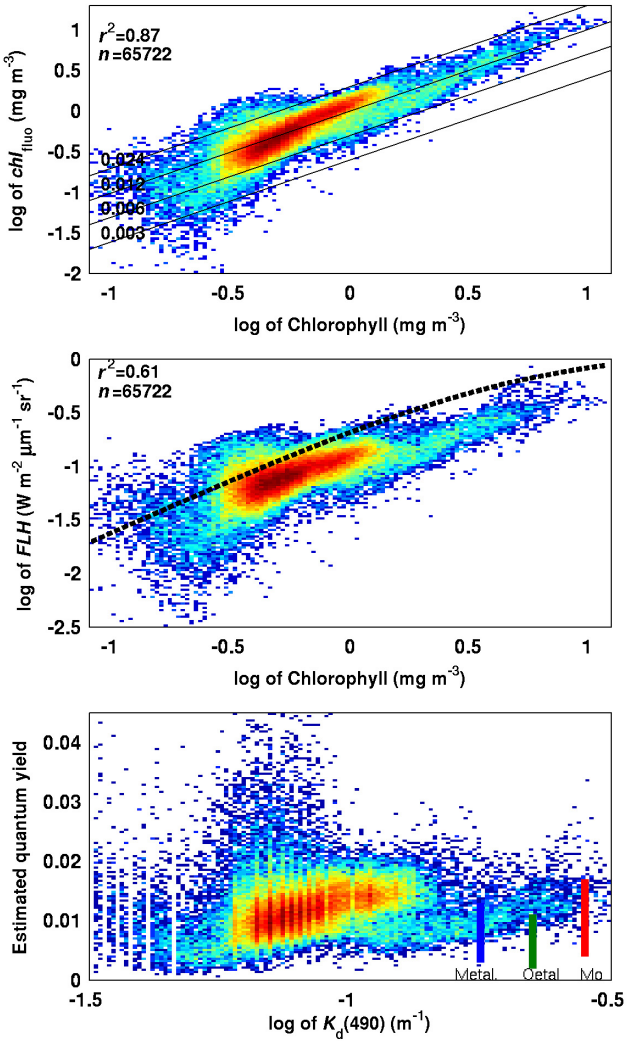

Fig. 13. Top panel: Comparison of our fluorescence estimate of the chlorophyll concentration, $chl_{fluo} = FLH \cdot \beta_{\varphi}/(\varphi_{chl} \cdot E_{PAR})$ (*see* Eqs. 8 and 14) with the MODIS chlorophyll product (chlor_a2, SeaWiFS analog chlorophyll algorithm). The middle panel is the comparison between *FLH* and chlorophyll concentration from MODIS. The dashed black line is the relationship derived by Gower et al. (2004), $FLH = 0.15 \cdot chl/(1 + 0.2 \cdot chl)$ multiplied by 1.65 to fit the data in Fig. 9. The bottom panel shows our retrieved quantum yield of fluorescence, φ_{est}, as a function of K_d (490). *See* Fig. 9 for more details.

is not observed in φ_{est}, which is much more uniform. As expected, the relationship between *CFE* and φ_{est} is weaker in this region (Fig. 15, top left). A small fraction of the points follows the trend line reproduced from Fig. 11, but otherwise the scatter is large. In contrast to Fig. 11 from off the coast of Central America, Fig. 15 shows strong dependence of the ratio of φ_{est}/CFE versus K_d (490), a_{gilvin} and *ARP*, which clearly shows that one of the yields is biased with respect to these retrieved optical properties. Fig. 16 highlights the resemblance between the map of MODIS retrieved a_{gilvin} and the ratio of CFE/φ_{est} consistent with a strong influence of the upwelling radiance at 412 nm on the relationship.

The same inverse model (Carder et al. 1999*a*; Carder et al. 1999*b*) is used to retrieve a_{φ} for the computation of *ARP* and to estimate a_{gilvin}. Our experience with such models, particularly implementations similar to that of Roesler and Perry (1995), has shown that generally an overestimate of a_{gilvin} leads to an underestimate of a_{φ} and vice-versa. An inverse pattern to the retrieved a_{gilvin} is observed in the normalized water - leaving radiance at 412 nm (lower 412 radiance where higher a_{gilvin} is present), and to a lesser extent at 443, but is not observed at 488 nm (data not shown). Along the high *CFE* line in Fig. 12, the *ARP* algorithm probably underestimated the phytoplankton absorption while at the same time overestimated the absorption by gilvin, leading to an overestimate of *CFE*. Whether the origin of this effect is in the atmospheric correction or the *ARP* model, we have not investigated.

Discussion

Quantum yield of fluorescence—Off the coast of Central America, the *CFE* was on average 58% lower than φ_{est}. Our estimate accounts for 76% of the variance found in the *CFE* (Fig. 11), and the maps of φ_{est} (Fig. 10) and *CFE* (Fig. 8) show similar patterns. In this region, the quantum yields compare well and a map of either would lead to the same interpretation. It is outside the scope of this paper to attribute the different quantum yields inside and outside the Costa Rica Dome area to physiological or physical processes, and we will merely speculate that likely candidates include different nutrient regimes, light acclimation states (for example, due to different mixing layer depths and attenuation coefficients, e.g., Field et al. 1998), or dominance by small cells (Li et al. 1983, leading to an underestimate of absorption and overestimate of the quantum yield) in the upwelling region. The strong difference between patterns in φ_{aQ}, whose variability includes effects of all physiological variables ($\varphi \cdot \bar{a}_{\varphi}^{*} \cdot Q_a^{*}$), and φ_{est}, which attempts to retrieve only φ, clearly emphasizes the importance of the term $\bar{a}_{\varphi}^{*} \cdot Q_a^{*}$ when retrieving the quantum yield of fluorescence. In fact, the much-reduced amplitude of φ_{aQ} compared to φ_{est} points to a strong effect of $\bar{a}_{\varphi}^{*} \cdot Q_a^{*}$ on the patterns observed in this region, whether it is an artifact due to our parameterization, or real.

Comments and recommendations

Chlorophyll and absorption as proxies for phytoplankton abundance—Because intra-cellular fluorescence emission is the product of the absorption of light by all phytoplankton pigments and the quantum yield as defined here (absorption by photoprotective pigments leads to a reduced quantum yield, e.g., Kiefer and Reynolds 1992; Gilmore and Govindjee 1999), phytoplankton absorption rather than chlorophyll is the better measure of biomass for fluorescence work. We use chlorophyll in our quantum yield model due to the lack of empirical models relating the blue-to-green ratio directly to absorption. Presently, the only algorithms to retrieve phytoplankton absorption from satellite ocean color are based on inverse mod-

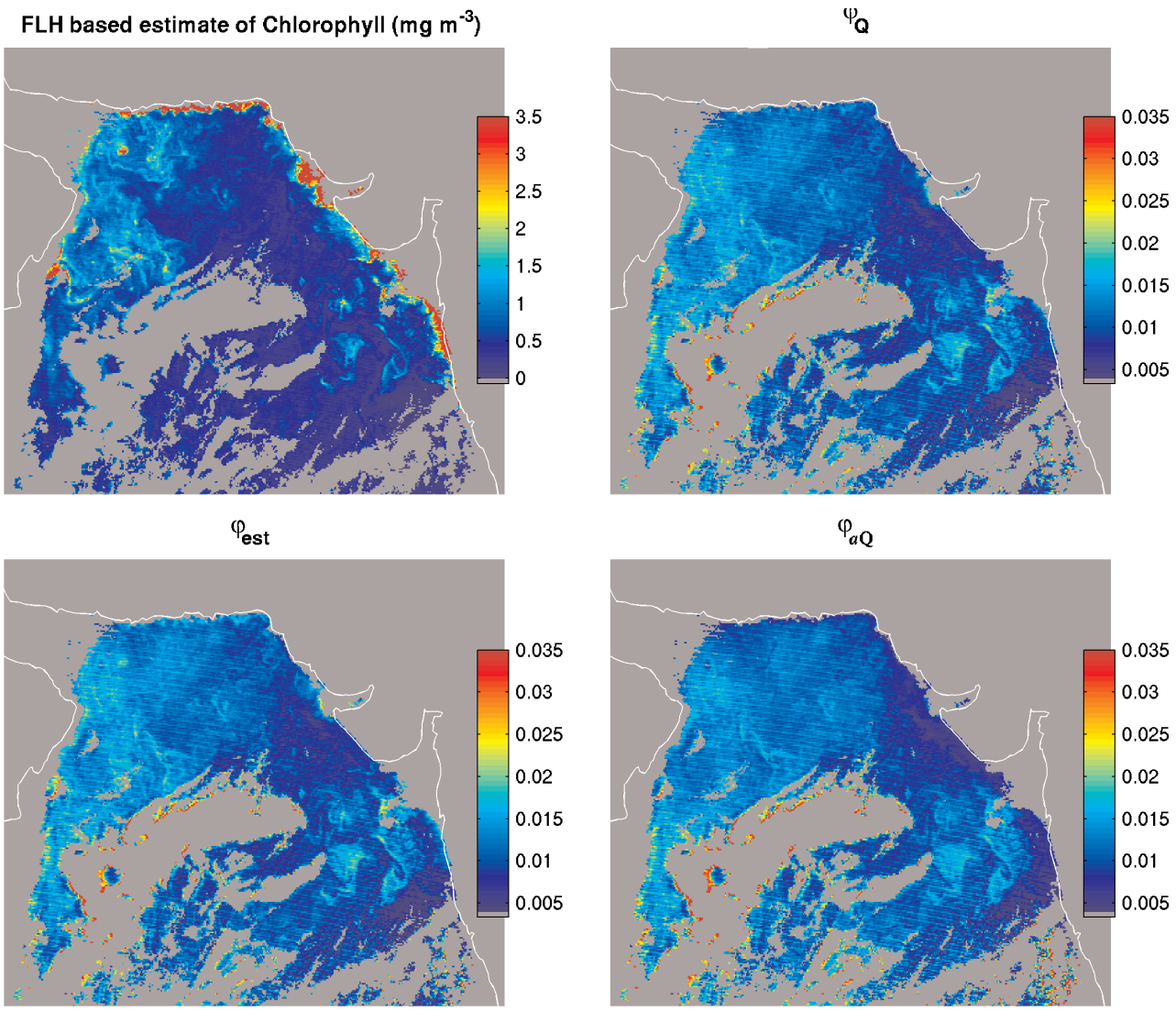

Fig. 14. Map of derived products for the Arabian Sea. *See* Fig. 10 for more details.

els (Carder et al. 1999*b*; Maritorena et al. 2002). As such, a future improvement of our quantum yield algorithm would be the use of an empirical algorithm retrieving $\bar{a}_\varphi$ and $a_\varphi(678)$ directly from the blue-to-green ratio. This would eliminate the need for an independent chlorophyll estimate and the relationships between $\bar{a}_\varphi^*$ and $a_\varphi(678)$ versus $K_d(490)$ to retrieve φ_{est}. Our chlorophyll algorithm could also be recast to retrieve phytoplankton absorption with higher accuracy. It would, however, be harder to validate and a less desirable product in the context of our focus on the retrieval of chlorophyll concentration.

Using chlorophyll instead of phytoplankton absorption, however, makes our algorithm very sensitive to its accurate retrieval. The estimate of φ_{est} for the same regions using the two other MODIS chlorophyll algorithms (Fig. 17, *see* Procedures) shows clear differences in the maps when compared with Fig. 10 and Fig. 14. The patterns observed are strongly influenced by the chlorophyll algorithm, and the physiological interpretation of these patterns would certainly be different. When using our quantum yield algorithm, we recommend using the chlorophyll algorithm that is best-suited for the region and time studied. As an example, note the reappearance of the stripe in the Arabian Sea region when using the semi-analytical (case 2) algorithm underlying the *ARP* model (Fig. 17).

The use of chlorophyll and a parameterization based on $K_d(490)$ has a further limitation for the retrieval of the quantum yield: if the remote-sensing algorithms used to retrieve $K_d(490)$ and chlorophyll do not follow the statistical relationships used (Bricaud et al. 1995; Morel and Maritorena 2001), it could lead to a bias in the retrieval of the yield. Presently, this could lead to errors of ~30% (sensitivity analysis not shown). This should not be a major limitation, and as algorithms evolve they will likely converge.

Validation of algorithms—Our algorithm and the MODIS *CFE* algorithm remain to be validated by measuring the quantum

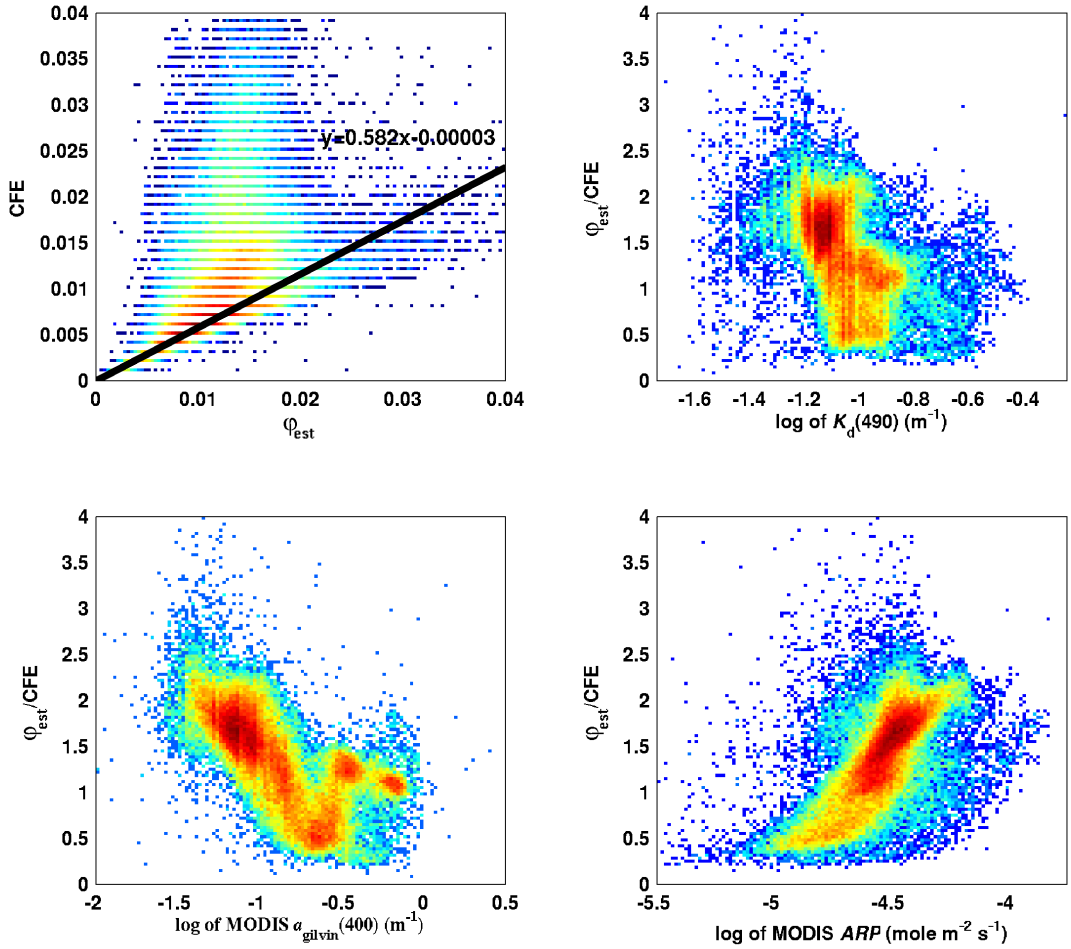

Fig. 15. Comparison of quantum yields for the Arabian Sea. *See* Fig. 11 for more details. Line in the upper left panel is the best fit from the upper left panel in Fig. 11.

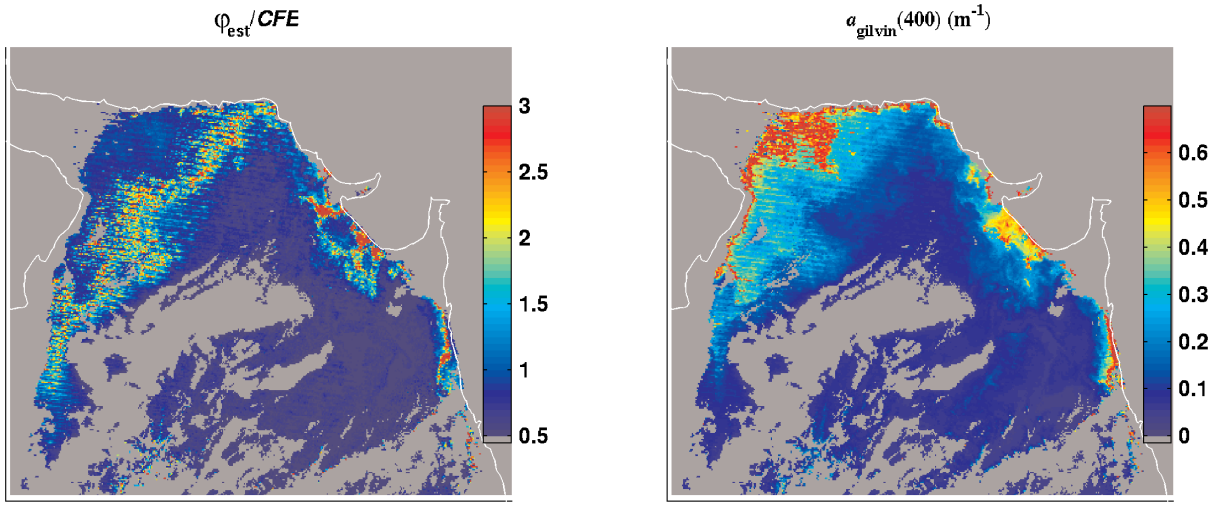

Fig. 16. The left panel is the ratio of the quantum yields while the right panel is the gilvin absorption at 400 nm as estimated by MODIS for the two study regions. Note the correspondence of the region with high φ_{est}/*CFE* with the transition region to higher a_{gilvin}.

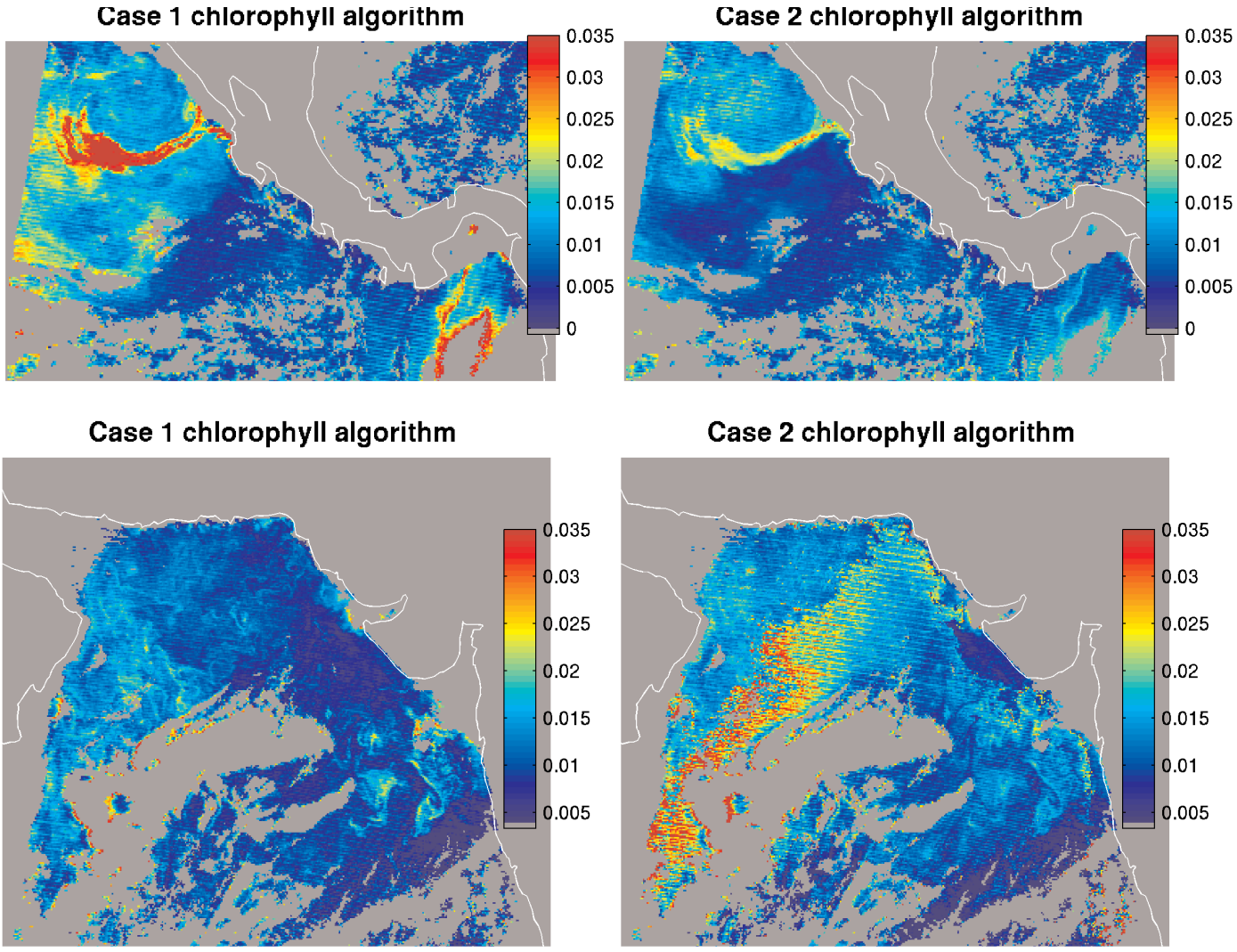

Fig. 17. Effect of different chlorophyll algorithms on the estimate of φ_{est}. Left column shows the results using the case 1 pigment algorithm (MOD 19), which provides an estimate of chlorophyll *a* and phaeopigments in case 1 waters. This algorithm is based on an empirical function of the ratio of blue-to-green water leaving radiance. The right column shows the application of the case 2 chlorophyll algorithm (MOD 21). The top row is for the subscene off the west coast of Central America, and the bottom row is the Arabian Sea subscene.

yield in situ under remote-sensing conditions. The conditions under which the MODIS data are collected are very consistent. It is always at the surface, under high irradiances, within 1 to 1.5 hour of the satellite's equatorial crossing time, and subject to large spatial averaging due to its resolution. This is a narrow set of conditions compared to those encountered when taking measurements at sea. As such, field validation of fluorescence algorithms will require great care. The time of sampling and the incident irradiance will have to match those encountered by the MODIS sensor, otherwise, the time and irradiance dependence of φ will affect the results (e.g., Morrison 2003).

Summary—We developed new methods to estimate the chlorophyll concentration and the quantum yield of fluorescence, incorporating the effects of pigment packaging on fluorescence emission and replacing the *ARP* algorithm used in MODIS *CFE* estimates with a different estimate of absorbed radiation, integrated to infinite depth. The new method seems robust, showing good agreement with MODIS chlorophyll and *CFE* estimates, and is apparently less sensitive to two artifacts:

(1) It will not be affected by a poor estimate of upwelling radiance at 412 nm as it does not rely on the semi-analytical absorption algorithm, which requires the 412 nm radiance to retrieve the absorption coefficients.

(2) The new method estimates absorbed radiation integrated to infinity, avoiding a bias in the MODIS *CFE* due to an incomplete account of the attenuation of incident irradiance.

The quantum yield estimate is, however, highly dependent on the retrieval of accurate chlorophyll concentration.

Conclusion—MODIS fluorescence products are relatively new, and like early chlorophyll images from the Coastal Zone

Color Scanner (CZCS), they bear tremendous promise. At present, they are still experimental, and issues such as accurate estimates of ipar and *ARP*, correction of the *FLH* measurement for the baseline, and proper depth integration need to be resolved. Only when these issues are settled can we assess whether the quantum yield of fluorescence under remote-sensing conditions provides a measure of phytoplankton physiology on global scales.

References

Abbott, M. R., and R. M. Letelier. 1999. Algorithm theoretical basis document chlorophyll fluorescence (MODIS product number 20). NASA.

Allali, K., A. Bricaud, and H. Claustre. 1997. Spatial variations in the chlorophyll-specific absorption coefficient of phytoplankton and photosynthetically active pigments in the equatorial Pacific. J. Geophys. Res. 102:12413-12423.

Anonymous. 2002. MERIS product handbook. <http://envisat.esa.int/dataproducts/meris/CNTR.htm>

Babin, M., A. Morel, H. Claustre, A. Bricaud, Z. Kolber, and P. G. Falkowski. 1996*a*. Nitrogen- and irradiance-dependent variations of the maximum quantum yield of carbon fixation in eutrophic, mesotrophic and oligotrophic marine systems. Deep-Sea Res. I 43:1241-1272.

———, A. Morel, and B. Gentili. 1996*b*. Remote sensing of sea surface sun-induced chlorophyll fluorescence: consequences of natural variations in the optical characteristics of phytoplankton and the quantum yield of chlorophyll *a* fluorescence. Int. J. Remote Sens. 17:2417-2448.

Bartlett, J. S., K. J. Voss, S. Sathyendranath, and A. Vodacek. 1998. Raman scattering by pure water and seawater. Appl. Opt. 37:3324-3332.

Bidigare, R. R., M. E. Ondrusek, J. H. Morrow, and D. A. Kiefer. 1990. In vivo absorption properties of algal pigments, p. 290-302. *In Spinrad, R.W.* [eds.], Ocean Optics X SPIE.

———, B. B. Prézelin, and R. C. Smith. 1992. Bio-optical models and the problems of scaling, p. 175-212. *In* P. G. Falkowski and A. Woodhead [eds.], Primary productivity and biogeochemical cycling in the sea. Plenum Press.

Bricaud, A., M. Babin, A. Morel, and H. Claustre. 1995. Variability in the chlorophyll-specific absorption coefficients of natural phytoplankton: Analysis and parameterization. J. Geophys. Res. 100:13321-13332.

Campbell, D., H. Vaughan, A. K. Clarke, P. Gustafsson, and G. Öquist. 1998. Chlorophyll fluorescence analysis of cyanobacterial photosynthesis and acclimation. Microbiol. Mol. Biol. R. 62:667-683.

Carder, K. L. 2003. Terra chlorophyll *a* pigment concentration (Case 2 waters) Data quality summary. <http://modis-ocean.gsfc.nasa.gov/qa/terra/dataqualsum/>

———, F. R. Chen, and S. K. Hawes. 2003. Algorithm theoretical basis document ATBD 20: Instantaneous photosynthetically available radiation and absorbed radiation by phytoplankton version 7. NASA.

———, F. R. Chen, Z. Lee, and S. K. Hawes. 1999*a*. Algorithm theoretical basis document ATBD 19 case 2 chlorophyll *a*. NASA.

———, F. R. Chen, Z. P. Lee, S. K. Hawes, and D. Kamykowski. 1999*b*. Semianalytic moderate-resolution imaging spectrometer algorithm for chlorophyll *a* concentration and absorption with bio-optical domains based on nitrate-depletion temperatures. J. Geophys. Res. 104:5403-5421.

Ciotti, Á. M., J. J. Cullen, and M. R. Lewis. 1999. A semi-analytical model of the influence of phytoplankton community structure on the relationship between light attenuation and ocean color. J. Geophys. Res. 104:1559-1578.

———, M. R. Lewis, and J. J. Cullen. 2002. Assessment of the relationship between dominant cell size in natural phytoplankton communities and the spectral shape of the absorption coefficient. Limnol. Oceanogr. 47:404-417.

Clark, D. K. 1999. Algorithm theoretical basis document ATBD 18 case 1 waters. NASA.

———. 2001. Terra-diffuse attenuation coefficient at 490 nm (K490) data quality summary. <http://modis-ocean.gsfc.nasa.gov/qa/terra/dataqualsum/>

Cleveland, J. S., and M. J. Perry. 1987. Quantum yield, relative specific absorption and fluorescence in nitrogen-limited *Chaetoceros gracilis*. Mar. Biol. 94:489-497.

Coleman, J. E., R. A. Reynolds, M. C. Talbot, M. Twardowski, and M. J. Perry. 2000. Utilization of solar-induced chlorophyll *a* fluorescence as an indicator of phytoplankton biomass in coastal waters. Ocean Optics XV.

Collins, D. J., D. A. Kiefer, J. B. Soohoo, and I. S. McDermid. 1985. The role of reabsorption in the spectral distribution of phytoplankton fluorescence emission. Deep-Sea Res. 32: 983-1003.

Cullen, J. J., and M. R. Lewis. 1995. Biological processes and optical measurements near the sea-surface: some issues relevant to remote sensing. J. Geophys. Res. 100:13255-13266.

——— and J. G. MacIntyre. 1998. Behavior, physiology and the niche of depth-regulating phytoplankton, p. 559-580. *In* D. M. Anderson, A. D. Cembella, and G. M. Hallegraeff [eds.], Physiological ecology of harmful algal blooms. Springer-Verlag.

Culver, M. E., and M. J. Perry. 1997. Calculation of solar-induced fluorescence in surface and subsurface waters. J. Geophys. Res. 102(C5):10563-10572.

Dandonneau, Y., and J. Neveux. 1997. Diel variations of the in vivo fluorescence in the eastern equatorial Pacific: an unvarying pattern. Deep-Sea Res. II 44:1869-1880.

Esaias, W. E., and others. 1998. An overview of MODIS capabilities for ocean science observations. IEEE T. Geosci. Remote 36:1250-1265.

Falkowski, P. G., and Z. Kolber. 1995. Variations in chlorophyll fluorescence yields in phytoplankton in the world oceans. Aust. J. Plant Physiol. 22:341-355.

Fell, F., E. Dilligeard, C. Olbert, M. Babin, and G. M. Ferrari. 2000. Using the sun-induced chlorophyll fluorescence for the remote

retrieval of phytoplankton in case-II waters: a case study. *In* S. Ackelson [ed.], Ocean Optics XV Office of Naval Research.

Fiedler, P. C. 2002. The annual cycle and biological effects of the Costa Rica dome. Deep-Sea Res. I 49:321-338.

Field, C. B., M. J. Behrenfeld, J. T. Randerson, and P. G. Falkowski. 1998. Primary production of the biosphere: Integrating terrestrial and oceanic components. Science 281:237-240.

Fisher, J., and U. Kronfeld. 1990. Sun-stimulated chlorophyll fluorescence 1: Influence of oceanic properties. Int. J. Remote Sens. 11:2125-2147.

Fournier, G. R., and J. L. Forand. 1994. Analytic phase function for ocean water, p. 194-201. *In* J. Jaffe [ed.], Ocean Optics XII. SPIE.

Gilmore, A. M., and Govindjee. 1999. How higher plants respond to excess light: Energy dissipation in photosystem II, p. 513-548. *In* G. S. Singhal, R. Renger, S. K. Sopory, K.-D. Irrgang, and Govindjee [eds.], Concepts in photobiology: photosynthesis and photomorphogenesis. Narosa-Publishing.

Gordon, H. R. 1979. Diffuse reflectance of the ocean: the theory of its augmentation by chlorophyll *a* fluorescence. Appl. Opt. 21:2489-2492.

———. 2002. Terra normalized water-leaving radiance data quality summary. <http://modis-ocean.gsfc.nasa.gov/qa/terra/dataqualsum/>

Gower, J. F. R., L. Brown, and G. A. Borstad. 2004. Observations of chlorophyll fluorescence in west coast waters of Canada using the MODIS satellite sensor. Can. J. Remote Sens. 30:17-25.

———, R. Doerffer, and G. A. Borstad. 1999. Interpretation of the 685 nm peak in water-leaving radiance spectra in terms of fluorescence, absorption and scattering, and its observation by MERIS. Int. J. Remote Sens. 20:1771-1786.

Gregg, W. W., and K. L. Carder. 1990. A simple spectral solar irradiance model for cloudless maritime atmosphere. Limnol. Oceanogr. 35:1657-1675.

Heaney, S. I. 1978. Some observations on the use of the in vivo fluorescence technique to determine chlorophyll *a* in natural populations and cultures of freshwater phytoplankton. Freshwater Biol. 8:115-126.

Ibelings, B. W., B. M. A. Kroon, and L. R. Mur. 1994. Acclimation of photosystem II in a cyanobacterium and a eukariotic green alga to high and fluctuating photosynthetic photon flux densities, simulating light regimes induced by mixing in lakes. New Phytol. 128:407-424.

Jeffrey, S. W., R. F. C. Mantoura, and S. W. Wright. 1997. Phytoplankton pigments in oceanography, p. 661. In [eds.], Monographs on oceanographic methodology. Unesco Publishing.

Johnsen, G., B. B. Prézelin, and R. V. M. Jovine. 1997. Fluorescence excitation spectra and light utilization in two red tide dinoflagellates. Limnol. Oceanogr. 42:1166-1177.

——— and E. Sakshaug. 1996. Light harvesting in bloom-forming marine phytoplankton: species specificity and photoacclimation. Sci. Mar. 60:47-56.

Kiefer, D. A. 1973. Chlorophyll *a* fluorescence in marine centric diatoms: responses of chloroplasts to light and nutrient stress. Mar. Biol. 23:39-46.

——— and R. A. Reynolds. 1992. Advances in understanding phytoplankton fluorescence and photosynthesis, p. 155-174. *In* P. G. Falkowski [ed.], Primary productivity and biogeochemical cycles in the sea. Plenum Press.

Kirk, J. T. O. 1994. Light and photosynthesis in aquatic ecosystems, 2nd ed. Cambridge Univ. Press.

Kolber, Z., and P. G. Falkowski. 1993. Use of active fluorescence to estimate phytoplankton photosynthesis in situ. Limnol. Oceanogr. 38:1646-1665.

Krause, G. H., and E. Weis. 1991. Chlorophyll fluorescence: The basics. Ann. Rev. Plant Physiol. 42:313-349.

Letelier, R., and M. R. Abbott. 1996. An analysis of chlorophyll fluorescence algorithms for the Moderate Resolution Imaging Spectrometer (MODIS). Remote Sens. Environ. 58:215-223.

Li, W. K. W., D. V. Rao, J. C. Harrison, J. C. Smith, J. J. Cullen, B. Irwin, and T. Platt. 1983. Autotrophic picoplankton in the tropical ocean. Science 219:292-295.

Loftus, M. E., and H. H. Seliger. 1975. Some limitations of the in vivo fluorescence technique. Chesapeake Sci. 16:79-92.

Long, S. P., S. Humphries, and P. G. Falkowski. 1994. Photoinhibition of photosynthesis in nature. Annu. Rev. Plant Phys. 45:633-662.

Lutz, V. A., S. Sathyendranath, E. J. H. Head, and W. K. W. Li. 1998. Differences between in vivo absorption and fluorescence excitation spectra in natural samples of phytoplankton. J. Phycol. 34:214-227.

———. 2001. Changes in the in vivo absorption and fluorescence excitation spectra with growth irradiance in three species of phytoplankton. J. Plankton Res. 23:555-569.

Maritorena, S., A. Morel, and B. Gentili. 2000. Determination of the fluorescence quantum yield by oceanic phytoplankton in their natural habitat. Appl. Opt. 39:6725-6737.

———, D. A. Siegel, and A. R. Peterson. 2002. Optimization of a semianalytical ocean color model for global-scale applications. Appl. Opt. 41:2705-2714.

McClain, C. R., J. R. Christian, S. R. Signorini, M. R. Lewis, I. Asanuma, D. Turk, and C. Dupouy-Douchement. 2002. Satellite ocean-color observations of the tropical Pacific Ocean. Deep-Sea Res. II 49:2533-2560.

Morel, A. 1978. Available, usable, and stored radiant energy in relation to marine photosynthesis. Deep-Sea Res. 25:673-687.

———. 1988. Optical modeling of the upper ocean in relation to its biogenous matter content (case 1 waters). J. Geophys. Res. 93:10749-10768.

———, D. Antoine, and B. Gentili. 2002. Bidirectional reflectance of oceanic waters: accounting for Raman emission and varying particle scattering phase function. Appl. Opt. 41:6289-6306.

——— and A. Bricaud. 1981. Theoretical results concerning light absorption in a discrete medium, and application to specific absorption of phytoplankton. Deep-Sea Res. 28:1375-1393.

———. and A. Bricaud. 1986. Inherent properties of algal cells including picoplankton: Theoretical and experimental results. *In* T. Platt and W. K. W. Li [eds.], Photosynthetic picoplankton. Can. Bull. Fish. Aquat. Sci. 214:521-559.

——— and B. Gentili. 1996. Diffuse reflectance of oceanic waters. III. Implication of bidirectionality for the remote-sensing problem. Appl. Opt. 35:4850-4862.

——— and S. Maritorena. 2001. Bio-optical properties of oceanic waters: A reappraisal. J. Geophys. Res. 106:7163-7180.

——— and L. Prieur. 1977. Analysis of variations in ocean color. Limnol. Oceanogr. 22:709-722.

Morrison, J. R. 2003. In situ determination of the quantum yield of phytoplankton chlorophyll *a* fluorescence: a simple algorithm, observations, and a model. Limnol. Oceanogr. 48:618-631.

Mueller, J. L. 2000. SeaWiFS algorithm for the diffuse attenuation coefficient, K(490), using water-leaving radiances at 490 and 555 nm, p. 24-27. *In* S. B. Hooker and E. R. Firstone [eds.], Seawifs postlaunch calibration and validation analyses. NASA GSFC.

Müller, P., X.-P. Li, and K. K. Niyogi. 2001. Non-photochemical quenching. A response to excess light energy. Plant Physiol. 125:1558-1566.

O'Reilly, J. E., and others. 1998. Ocean color chlorophyll algorithm for SeaWiFS. J. Geophys. Res. 103:24.937-924.953.

Ögren, E. 1994. The significance of photoinhibition for photosynthetic productivity, p. 433-447. *In* W. J. Davies [ed.], Photoinhibition of photosynthesis from molecular mechanisms to the field. Environmental Plant Biology. BIOS Scientific Publisher.

Ostrowska, M., M. Darecki, and B. Wozniak. 1997. An attempt to use measurements of sun-induced chlorophyll fluorescence to estimate chlorophyll *a* concentration in the Baltic Sea. Proceedings of SPIE, International Society of Optical Engineering 3222:528-537.

Pope, R. M., and E. S. Fry. 1997. Absorption spectrum (380-700 nm) of pure water. II. Integrating cavity measurements. Appl. Opt. 36:8710-8723.

Pospisil, P. 1997. Mechanisms of non-photochemical chlorophyll fluorescence quenching in higher plants. Photosynthetica 34:343-355.

Preisendorfer, R. W., and C. D. Mobley. 1988. Theory of fluorescent irradiance fields in natural waters. J. Geophys. Res. 93:10831-10855.

Roesler, C. S., and M. J. Perry. 1995. In situ phytoplankton absorption, fluorescence emission, and particulate backscattering spectra determined from reflectance. J. Geophys. Res. 100:13279-13294.

Salomonson, V. 2004. MODIS Characterization Support Team (MCST) Web page http://www.mcst.ssai.biz/mcstweb/

Sosik, H. M., and B. G. Mitchell. 1995. Light absorption by phytoplankton, photosynthetic pigments and detritus in the California Current System. Deep-Sea Res. I 42:1717-1748.

Submitted 13 May 2004
Revised 15 October 2004
Accepted 26 October 2004